JGR Atmospheres

RESEARCH ARTICLE
10.1029/2021JD034888

Emissions of Tetrafluoromethane (CF_4) and Hexafluoroethane (C_2F_6) From East Asia: 2008 to 2019

Jooil Kim[1], Rona Thompson[2], Hyeri Park[3], Stephanie Bogle[4], Jens Mühle[1], Mi-Kyung Park[5], Yeaseul Kim[6], Christina M. Harth[1], Peter K. Salameh[1], Roland Schmidt[1], Deborah Ottinger[4], Sunyoung Park[3], and Ray F. Weiss[1]

[1]Scripps Institution of Oceanography, University of California San Diego, La Jolla, CA, USA, [2]Norwegian Institute for Air Research (NILU), Kjeller, Norway, [3]Department of Oceanography, Kyungpook National University, Daegu, Republic of Korea, [4]Climate Change Division, Office of Atmospheric Programs, Environmental Protection Agency, Washington, DC, USA, [5]Kyungpook Institute of Oceanography, Kyungpook National University, Daegu, Republic of Korea, [6]School of Earth System Sciences, Kyungpook National University, Daegu, Republic of Korea

Abstract The perfluorocarbons (PFCs), tetrafluoromethane (CF_4) and hexafluoroethane (C_2F_6), are potent greenhouse gases with very long atmospheric lifetimes. They are emitted almost entirely from industrial sources, including the aluminum and rare earth metal smelting industries that emit them as by-products, and the semiconductor and flat panel display manufacturing industries that use them and vent unutilized amounts to the atmosphere. Despite extensive industrial efforts to quantify and curb these emissions, "top-down" PFC emission estimates derived from atmospheric measurements continue to rise and are significantly greater than reported process- and inventory-based "bottom-up" emissions. In this study, we estimate emissions of CF_4 and C_2F_6 from East Asia, where PFC emitting industries are heavily concentrated, using a top-down approach (a Bayesian inversion) with high-frequency atmospheric measurements at Gosan (Jeju Island, South Korea) for 2008–2019. We also compile and analyze the available bottom-up CF_4 and C_2F_6 emissions in East Asia from industrial and government reports. Our results suggest that the observed increases in global PFC emissions since 2015 are driven primarily by China's aluminum industry, with significant contributions from Japan's and Korea's semiconductor industry. Our analysis suggests that Chinese emissions occur predominantly from the aluminum industry, although their emissions per production ratio may be improving. Our results for Japan and Korea find significant discrepancies between top-down and bottom-up emissions estimates, suggesting that the effectiveness of emission reduction systems (abatement) used in their semiconductor industries may be overestimated. Overall, our top-down results for East Asia contribute significantly to reducing the gap in the global PFC emission budgets.

Plain Language Summary CF_4 and C_2F_6, emitted mainly from the aluminum and semiconductor industries, are some of the longest-lived greenhouse gases known, and among the compounds included under the United Nations Framework Convention on Climate Change in the global effort to reduce greenhouse gas emissions and mitigate climate change. Despite significant progress from both industries in understanding and reducing their emissions over the last 3 decades, the global emissions of CF_4 and C_2F_6 modeled using atmospheric measurements continue to rise, and are significantly larger than those currently reported by industry and government. In this study, we estimate CF_4 and C_2F_6 emissions over 2008–2019 in East Asia, where the aluminum and semiconductor industries are heavily concentrated, using a regional inverse model framework combined with measurements at a site in East Asia (Gosan, Jeju Island, South Korea). Our results confirm the dominant role of East Asian emissions in the global budgets of CF_4 and C_2F_6, led by emissions from China's aluminum industry. Our regional emission estimates are significantly larger than those reported for this region, locating a significant source of the global discrepancy between the reported and atmospheric measurements based emissions for these compounds. We analyze key uncertainties that could lead to these discrepancies.

Key Points:

- CF_4 and C_2F_6 emissions in East Asia quantified using observations at Gosan (Jeju Island, South Korea) combined with Bayesian inverse model
- East Asian emissions, significantly underestimated in industry and government reports, drive the global emissions increase since 2015
- China's emissions dominated by aluminum industry, and significant uncertainties found in Japan and Korea's semiconductor industry emissions

Supporting Information:

Supporting Information may be found in the online version of this article.

Correspondence to:

J. Kim,
jjkim@ucsd.edu

Citation:

Kim, J., Thompson, R., Park, H., Bogle, S., Mühle, J., Park, M.-K., et al. (2021). Emissions of tetrafluoromethane (CF_4) and hexafluoroethane (C_2F_6) from East Asia: 2008 to 2019. *Journal of Geophysical Research: Atmospheres*, *126*, e2021JD034888. https://doi.org/10.1029/2021JD034888

Received 16 MAR 2021
Accepted 3 AUG 2021

Author Contributions:

Conceptualization: Jooil Kim, Jens Mühle, Ray F. Weiss
Data curation: Jooil Kim, Hyeri Park, Stephanie Bogle, Mi-Kyung Park, Christina M. Harth, Peter K. Salameh, Roland Schmidt
Formal analysis: Jooil Kim, Hyeri Park, Stephanie Bogle, Mi-Kyung Park, Yeaseul Kim

© 2021. The Authors.
This is an open access article under the terms of the Creative Commons Attribution-NonCommercial License, which permits use, distribution and reproduction in any medium, provided the original work is properly cited and is not used for commercial purposes.

1. Introduction

Tetrafluoromethane (CF_4, PFC-14, or CAS 75-73-0) and hexafluoroethane (C_2F_6, PFC-116, or CAS 76-16-4), are the two most abundant perfluorocarbons (PFCs) in the atmosphere (Hartmann et al., 2014; Mühle

Funding acquisition: Rona Thompson, Sunyoung Park, Ray F. Weiss
Investigation: Jooil Kim, Stephanie Bogle, Jens Mühle, Yeaseul Kim, Deborah Ottinger, Sunyoung Park
Methodology: Jooil Kim, Rona Thompson, Hyeri Park, Stephanie Bogle, Yeaseul Kim
Project Administration: Ray F. Weiss
Resources: Stephanie Bogle, Deborah Ottinger, Sunyoung Park
Software: Jooil Kim, Rona Thompson, Hyeri Park, Yeaseul Kim, Peter K. Salameh
Supervision: Sunyoung Park, Ray F. Weiss
Validation: Jooil Kim, Rona Thompson, Hyeri Park, Mi-Kyung Park, Christina M. Harth, Peter K. Salameh, Roland Schmidt
Visualization: Jooil Kim, Rona Thompson
Writing – original draft: Jooil Kim, Rona Thompson, Stephanie Bogle, Jens Mühle
Writing – review & editing: Jooil Kim, Rona Thompson, Hyeri Park, Stephanie Bogle, Jens Mühle, Deborah Ottinger, Sunyoung Park, Ray F. Weiss

et al., 2010; Trudinger et al., 2016). Moreover, they are both potent greenhouse gases (GHGs) with long atmospheric lifetimes, currently estimated at 50,000 and 10,000 years, respectively, leading to global warming potentials of 6,630 and 11,100, respectively, over a 100-year timescale (Myhre et al., 2013).

The primary aluminum smelting (AL) industry has been historically the largest source of PFCs, where electrolytic reduction is used to extract aluminum from aluminum oxide (alumina, Al_2O_3), and emissions occur during over-voltage conditions in the reduction cell due to restrictions in the feed of alumina and/or within the cell, referred to as "anode effects" (Holiday & Henry, 1959; IAI, 2020; Taberaux, 1994; Wong et al., 2015). These anode effect PFC emissions have been reported to be substantially reduced over time through process improvements (IAI, 2020; Marks & Bayliss, 2012). However, recent studies have also identified PFC emissions from previously unknown "low voltage anode effects" (Marks & Nunez, 2018; Ottinger & Cai, 2019; Wong et al., 2015), which are reported to be especially important for China's AL industry due to their unique design with large electrolytic reduction cells (Marks & Nunez, 2018), as we discuss in Section 3.1.

The rare earth metals smelting (RE) industry is another PFC source, as the electrolysis process is similar to that of the AL industry (Cai et al., 2018; Vogel & Friedrich, 2015). PFC emission estimates from this industry are currently highly uncertain with a wide range of potential emissions suggested in literature (Cai et al., 2018; Vogel & Friedrich, 2018), as we discuss in Section 3.3.

PFCs are used by the semiconductor (SC) manufacturing industry to produce plasmas for dry etching of wafers and to clean chemical vapor deposition chambers. PFC emissions occur primarily through two mechanisms. First, emissions occur when the supplied PFCs are not fully decomposed in plasma generation and then vent to the atmosphere. Second, by-product emissions (e.g., of CF_4) occur from decomposition of other fluorinated compounds fed into the process (Bartos et al., 2006; Ottinger & Cai, 2019). Calculating these emissions is complicated as usage rates (i.e., how much of the gas input is decomposed) and by-product formations rates vary significantly by compound, process, and among individual facilities. The SC industry has strived to reduce PFC emissions since the 1990s, mainly by replacing PFCs with alternatives (e.g., NF_3 instead of C_2F_6 for chemical vaporization deposition chamber cleaning), and by implementing abatement technologies to destroy PFCs in facility waste gas streams (Arnold et al., 2013; Chang & Chang, 2006; Czerniak, 2018; WSC, 2020). Similar processes lead to PFC emissions from flat panel display (FPD) manufacturing, but their reported consumption and emissions of CF_4 and C_2F_6 are comparatively small (as we discuss in Sections 2 and 3.2).

Other minor industrial emission sources for PFCs include vented and leaked emissions from fluorochemical production, and uses in circuit board waterproofing, photo-voltaic cell manufacture, and refrigerant applications (Bogle & Ottinger, 2020). CF_4 is also emitted from the Earth's lithosphere, leading to a natural atmospheric background (Deeds et al., 2008; Harnisch & Eisenhauer, 1998; Mühle et al., 2010; Trudinger et al., 2016), but these emissions occur on geological time scales and are negligible compared to the industrial sources.

Measurements of the Advanced Global Atmospheric Gases Experiment (AGAGE) have documented the global increase in atmospheric concentrations of CF_4 and C_2F_6 over the last few decades (Mühle et al., 2010; Prinn et al., 2018; Trudinger et al., 2016). "Top-down" (TD) estimates of PFC emissions, derived from combining these global measurements with atmospheric transport models, are significantly higher than the reported "bottom-up" (BU) emissions derived from activity data (e.g., consumption, production, anode effect occurrences) and corresponding emission factors for each of the industrial sources (Kim et al., 2014; Mühle et al., 2010). Kim et al. (2014) further analyzed the global TD versus BU discrepancy using distinct C_2F_6/CF_4 emission ratios for the AL and SC industries, and reported that the increasing discrepancy since 2003 is likely connected to the significant growth in China's AL industry. In addition, the latest results of the global TD emissions for CF_4 and C_2F_6 (Say et al., 2021) suggest a significant increase in emissions since 2015 for both PFCs (as we discuss in Section 2).

In this analysis of CF_4 and C_2F_6 emissions from East Asia we address some of the discrepancies and uncertainties identified in these previous studies. A substantial portion of global industrial sources are concentrated in East Asia, with China now estimated to account for 55% of global AL production (IAI, 2020) and 80% of global RE production (Smith, 2020), while China, Japan, South Korea (Korea), and Taiwan are dominant entities in the global SC industry accounting for 66% of the global production capacity in 2011

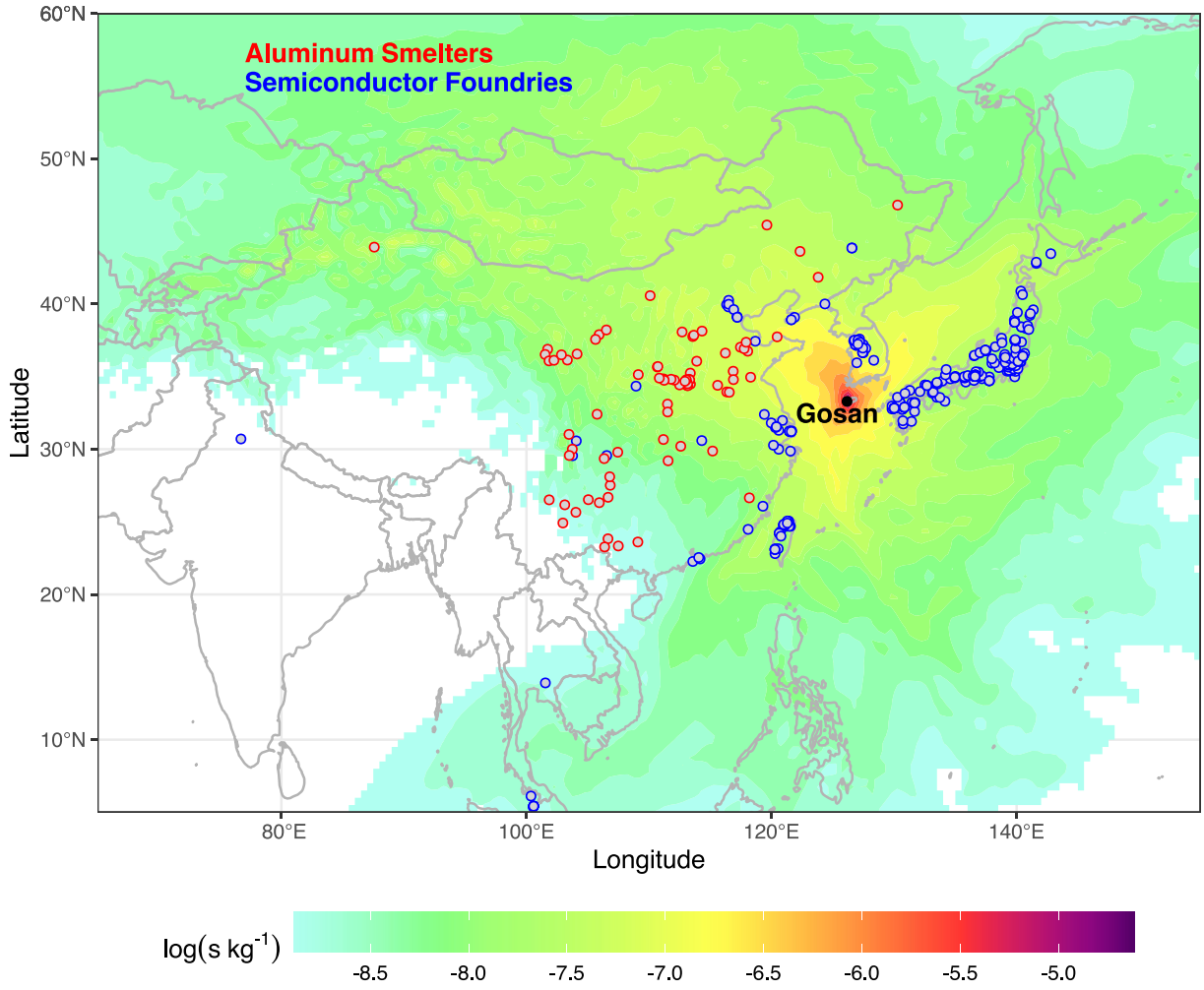

Figure 1. Map of East Asia, the regional focus of this study, with Gosan station (Jeju Island, Korea), the measurement site used in this study, shown in black. Also shown in dots are locations of aluminum smelters, in red, researched for this study (see discussions in Section 4.3.1), and semiconductor foundry locations, in blue, adopted from Mühle et al. (2019). Color scale represents transport model sensitivities estimated using FLEXPART for 2008 to Gosan (see Section 4.2 for details).

(IC Insights, 2011). AGAGE observations at the Gosan station (Jeju Island, Korea, Figure 1) are ideal for deriving TD regional emissions of halogenated trace gases in East Asia (Arnold et al., 2018; Fang, Park, et al., 2019; Fang, Yao, et al., 2019; Kim et al., 2010; Li et al., 2011; Mühle et al., 2019; Park et al., 2021; Rigby et al., 2019; Stohl et al., 2010). We take a similar approach in applying a Bayesian inverse method (FLEXINVERT+) (Thompson & Stohl, 2014) to estimate TD emissions of CF_4 and C_2F_6 in East Asia. Our results are compared to BU emissions reported for China (IAI, 2020; Ottinger & Cai, 2019), Korea (GIR, 2020), and Japan (GIO, 2020) to assess TD versus BU discrepancies on these regional scales, and put into the global context with comparisons to recent trends in global TD CF_4 and C_2F_6 emissions.

2. An Updated Look at the Discrepancies Between the Observation Based Top-Down and Inventory Based Bottom-Up Global Emissions Estimates of CF_4 and C_2F_6

To assess East Asia's role in the global budget discrepancies in CF_4 and C_2F_6 emissions, we first compile the global total TD and BU emissions of CF_4 and C_2F_6 as shown in Figure 2. The global TD emissions, derived from global background measurements in the AGAGE network combined with a 12-box model (Say et al., 2021), were relatively stable over 2008–2014, after which they substantially increased. Comparing

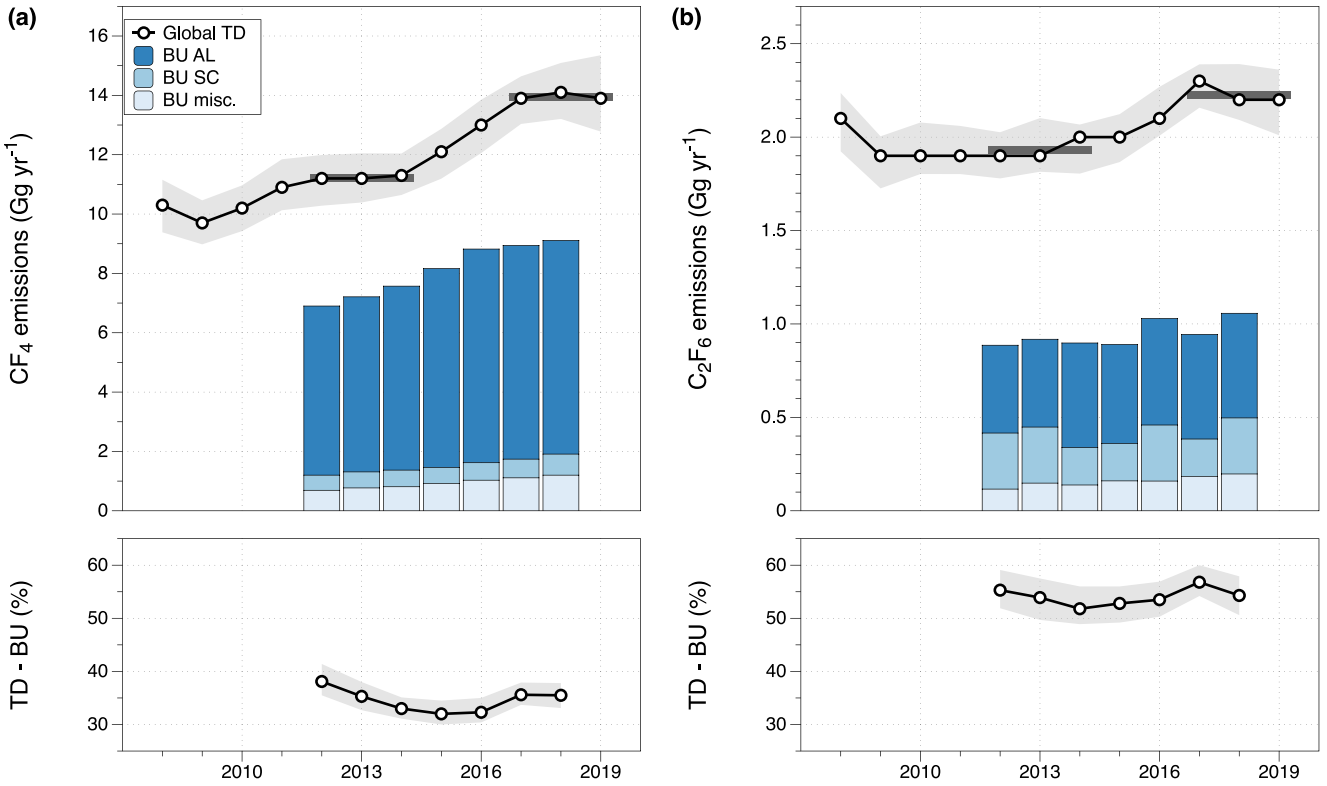

Figure 2. Global top-down and bottom-up (BU) emissions of (a) CF_4 and (b) C_2F_6, based on the Advanced Global Atmospheric Gases Experiment global 12-box model with uncertainties representing the sixteenth and eighty fourth percentiles of the model distribution (Say et al., 2021) and BU data for the aluminum industry (IAI, 2020; Ottinger & Cai, 2019; Bogle & Ottinger, 2020), semiconductor industry (WSC, 2020), and other miscellaneous sources (Bogle & Ottinger, 2020), see Section 2 and Table A1 for details.

2017–2019 to 2012–2014, the mean emissions increase by 2.71 ± 0.09 Gg yr^{-1} for CF_4 (+24 ± 1% from 2012 to 2014) and by 0.29 ± 0.15 Gg yr^{-1} for C_2F_6 (+15 ± 8% from 2012 to 2014).

The global BU emissions from AL industries in Figure 2 are derived from reports of the International Aluminum Institute (IAI, 2020), with additional corrections for low-voltage anode effect emissions and updated emission factors from the 2019 Refinement to the 2006 IPCC Guidelines for National Greenhouse Gas Inventories (Bogle & Ottinger, 2020; Ottinger & Cai, 2019).

The global SC industry BU emissions are from the World Semiconductor Council (WSC), representing the Semiconductor Industry Associations in China, Chinese Taipei, Europe, Japan, Korea and the United States. The totals include emissions from member SC companies in those regions as well as from member semiconductor companies in other regions (WSC, 2020). Some emissions are likely from SC manufacturers not associated with the WSC, but those emissions are currently difficult to estimate.

We also include estimated BU emissions from miscellaneous sources including the FPD industry, chemical production, circuit board waterproofing, and photo-voltaic cell (solar panel) manufacture, as reported by Bogle and Ottinger (2020). Of note, emissions from photo-voltaic cell manufacture, calculated with updated emission factors derived from manufacturing based in the United States, are estimated to have grown rapidly since 2005, and currently make up the largest portion among the miscellaneous sources in Figure 2.

Overall, these results suggest that over 2012%–2018%, 35% and 54% of the observed global TD emissions of CF_4 and C_2F_6, respectively, are not accounted in the reported global BU emissions, and that the global TD versus BU discrepancies are stable over time for both species, even as both emission estimates are increasing significantly. Annual global TD and BU emissions compiled for this study are listed in Table A1.

3. Reported Bottom-Up East Asian Emissions

3.1. China's Aluminum Industry Emissions From the International Aluminum Institute

3.1.1. General Methodology

Our BU estimates of China's AL industry PFC emissions are calculated based on reported production data from IAI (2020) by applying a reported emission factor of 0.161 kg CF_4 and 0.013 kg C_2F_6 per ton of aluminum produced (Ottinger & Cai, 2019). This emission factor was derived from a survey of 27 smelters in China in 2008–2013 (Marks & Nunez, 2018), and would take into account emissions from anode effects at both high and low voltages, being based on total emissions measured at the smelter exhausts. Of note, this emission factor is significantly larger than that reported for non-Chinese smelters (0.057 kg CF_4, 0.0068 kg C_2F_6 per ton of aluminum produced, over 2007–2019), while China's C_2F_6/CF_4 ratio as derived from the survey (0.081, by weight) is significantly smaller than that reported for non-Chinese smelters (0.119, by weight, over 2007–2019) (IAI, 2020). These differences likely stem from the specific aluminum smelter technologies used in China, based on modern large cells with more than 30 large anodes operating at high line currents exceeding 350 kA without fully automated anode effect intervention strategies for reducing PFC emissions. This design with high line currents can also lead to significantly larger low voltage anode effect emissions, which consists of CF_4 (Marks & Nunez, 2018; Ottinger & Cai, 2019).

China's AL industry emission estimates are more uncertain than those derived for most smelters outside China, because using a single production-based emission factor to estimate emissions (so-called Tier 1 method) is unlikely to represent the full variability of real-world emissions. Nearly all smelters outside China have incorporated measurements of parameters which are more directly representative of the anode conditions that lead to PFC emissions at each facility (e.g., over-voltage magnitudes and duration; so-called Tier 2 or 3 methods), likely leading to more accurate emission estimates (Bartos et al., 2006; IAI, 2020; Ottinger & Cai, 2019).

The Chinese AL industry emissions reported here are slightly higher than IAI's currently reported emissions as we adopted updated emission factors of the IPCC 2019 refinement, which derive larger emission factors based on the mean values of the 27-smelter survey (Ottinger & Cai, 2019), rather than the median values currently used by the IAI (IAI, 2020).

3.1.2. Aluminum Bottom-Up Results

Our analysis of the AL industry's reporting for the period of 2008–2019, shown in Figure B1 and Table B1, confirms the significant growth of China's AL industry and its dominant role in the global AL production and PFC emissions. China's AL production has grown at a rate of 13% per year between 2008 and 2016, followed by a plateau during 2017–2019. China's share of the global AL production over this period increased from 36% in 2008%–2010% to 56% in 2017–2019, and on average accounted for 49% of the total global production during 2008–2019. China's BU AL industry emissions account for 66% of the global BU AL industry total CF_4 and C_2F_6 emissions over 2008–2019, a significantly larger portion compared to China's share in global production, and these percentages increase to 81% and 83% for CF_4 and C_2F_6, respectively, when considering only 2017–2019.

3.2. Semiconductor and Flat Panel Display Emissions From the National Inventory Reports for Japan and Korea

3.2.1. General Methodology and Estimating Abatement

The National Inventory Reports (NIRs) of Japan (GIO, 2020) and Korea (GIR, 2020) are compiled in accordance with the United Nations Framework Convention on Climate Change and report BU estimates of emissions from each country's SC and FPD industries. One limitation is that industry emissions are not specified per compound, but instead aggregated as CO_2-equivalent quantities either by compound families (Japan) or as industry totals (Korea) and in the case for Korea since 2016, further aggregated to totals for the SC and FPD industries.

To address this, we take the compound-specific annual consumption amounts for the SC and FPD industries reported in the NIRs and estimate the specific emissions of CF_4 and C_2F_6 following the IPCC Tier 2 methodology (Bartos et al., 2006) used in the NIRs (GIO, 2020; GIR, 2020).

The general IPCC Tier 2 formula for the SC and FPD industries (Bartos et al., 2006) takes into account the significantly different utilization rates for each compound as well as different emission reductions from abatement to incinerate any unutilized amounts in the effluent:

$$E = \mathrm{FC} \times P \times \left(1 - U\right) \times A \tag{1}$$

where E is the BU emission per compound (Mg), FC is the consumed amount of each compound (Mg), P is the process supply rate taking into account the small amounts of compounds left in the gas cylinders at end-of-use (decimal range of 0–1, specified as 0.9). U is the specific utilization rate for each compound (the amount of PFC actually decomposed to a plasma, decimal range of 0–1). U can be specified for use case (etching or chemical vaporization deposition chamber cleaning) and per each facility, but lacking detailed data to apply these specific utilization rates, our study uses general compound-specific values for U. A is the fraction of the effluent not treated with abatement and released to the atmosphere, and can be further detailed as:

$$A = 1 - a \times d \tag{2}$$

where a is the fraction of the effluent processed with abatement equipment (decimal range of 0–1), and d is the destruction efficiency of the abatement equipment (decimal range of 0–1, specified as 0.9).

By-product emissions (BPE) (e.g., CF_4 emissions from use of C_2F_6) are known to make significant contributions to the total emissions, and are calculated using a formula similar to Equation 1:

$$\mathrm{BPE} = \mathrm{FC} \times B \times P \times A \tag{3}$$

where the U in Equation 1 is replaced with B, the by-production rate specified for each compound (decimal range of 0–1).

The value of A (the effective abatement rate) in both Equations 1 and 3 is a significant source of uncertainty in our compound-specific calculations, as it is currently not directly reported, and likely to have changed significantly over time. To assess this value from the reported data, we first calculate compound specific emissions assuming a is 0 (i.e., no abatement occurs, and A is 1), and refer to this estimate as "consumption based." We then estimate A for each year based on the following formula:

$$A = E_{\mathrm{co2eq}} \,/\, \sum_{i=1}^{N} E_i \times \left(\mathrm{GWP}_i\right) \tag{4}$$

where E_{co2eq} is the reported aggregated CO_2-equivalent emissions for each year, the variable i represents each of the N compounds that are included in the aggregation, and the E_i and GWP_i are the consumption-based emissions (i.e., emissions calculated assuming no abatement) and CO_2-equivalent GWPs of each compound, respectively. The number of compounds that are considered in Equation 4 can vary depending on the NIR reporting of the E_{co2eq}. For Japan, where E_{co2eq} is available specifically for PFCs, we consider the emissions of CF_4, C_2F_6, C_3F_8, and c-C_4F_8 in determining A. For Korea, where E_{co2eq} is reported for all consumed compounds, we also account for CHF_3, CH_2F_2, and SF_6 in the calculations. By applying the annual A derived from this method to the consumption-based emissions, we derive annual compound-specific emissions after abatement.

The reporting format in Korea's NIR has changed since 2016 to report CO_2 equivalent emissions for SC and FPD combined and so A for 2016 through 2018 in the SC industry cannot be directly calculated for those years. As such, we assume the 2015 value for A in 2016–2018, taking into account that the A calculated for the combined SC and FPD industries remains consistent from 2015 through 2018, as shown in Table B3.

Japan's NIR also reports PFC emissions from fugitive leaks during PFC production and recycling of cylinders at end-of-use, but as these emissions are reported only for all PFCs aggregated in CO_2-equivalent quantities, it is difficult to assess how these emissions impact our analysis. The NIR does note that significant emission reductions from this sector were achieved 2011 onwards due to installation of abatement equipment. Emissions from Japan's aluminum industry is reported to have been only about 1% or less of the

SC emissions with abatement, and zero since 2015, and thus is not considered here. The Korean NIR reports no aluminum production in Korea since 1990, while fugitive emissions from PFC production are stated to be likely, but not currently calculated due to lack of industry reported data.

3.2.2. Semiconductor Bottom-Up Results

Our estimates of BU emissions for Japan and Korea, both consumption-based and with abatement, along with estimated abatement rates for each country are detailed in Tables B2 (Japan) and B3 (Korea). Our results suggest that abatement is a significant factor in the reported CF_4 and C_2F_6 emissions, reducing Japan's SC emissions by 50% and FPD emissions by 86%, while reducing Korea's SC emissions by 31% and FPD emissions by 55%, on average over 2008–2018. Our results suggest that SC industry's abatement generally lags the abatement in the FPD industry. Also notable is that Korea's abatement has increased significantly in recent years. SC industry consumption and emissions are shown to be significantly larger than those of FPD industry in both countries, especially for C_2F_6 where consumption in the FPD industry has ceased since 2008 for Korea and 2013 for Japan.

The SC emissions derived in this study can be compared to the global consumption and emissions reported annually in the joint statements of the World Semiconductor Council (WSC, 2020), shown in Figure 2 and detailed in Table B4. For the period of 2012–2018 and taking into account our estimates for abatement, we find that the reported BU SC CF_4 emissions for Japan and Korea make up 70% of the reported global BU SC industry totals, based on consumption equal to 55% of the global totals. For C_2F_6 over the same period, our BU SC emissions (with abatement) in Japan and Korea make up only 29% of the global industry totals based on 34% of the global consumption, a smaller proportion of the global totals compared to CF_4. This may suggest that C_2F_6 phase-out for replacements such as NF_3 (Arnold et al., 2013; Czerniak, 2018; WSC, 2020) has progressed more in Japan and Korea compared to other regions. Overall, our results, with our accounting for abatement, are in reasonable agreement with the World Semiconductor Council's global report, which suggests that our estimates of abatement in Japan and Korea are in line with those assumed in the industry.

Comparing the reported BU emission quantities of the SC and FPD industries, we find that SC emissions account for 94% and 96% of total CF_4 emissions for Japan and Korea, respectively, and 100% for C_2F_6 in both countries, over 2008–2018, after accounting for abatement. This is due to a combination of significantly larger consumption of PFCs in the SC industry, especially for C_2F_6 which the FPD industry reports zero consumption since 2008 for Korea and 2013 for Japan, and higher adoption of abatement in the FPD industry (based on our analysis of abatement rates for both industries, refer to Tables B2 and B3 for details). As such, our analysis for Japan and Korea will focus on the SC industry, unless stated otherwise.

3.3. Other Sources of PFCs in East Asia

Current estimates of PFC emissions from China's RE industries are highly uncertain. While the general processes of PFC emissions are similar to those in the AL industry, an accurate assessment of the emission characteristics in the RE industry has been difficult, with the few existing studies finding a large range of possible emission factors (Cai et al., 2018; Vogel & Friedrich, 2018). Accurate accounting of total production is also difficult due to a substantial amount of illegal mining, estimated to be up to 45% of the legally reported mining (and production) in one study (Vogel & Friedrich, 2018). Combined, the estimated emissions reported range from being insignificant to more than 100% of the global TD emission totals (Vogel & Friedrich, 2018). Further efforts to constrain these emissions from BU are beyond the scope of this study. Also, the PFC emissions from China's SC and FPD industries, while certain to exist, are difficult to estimate due to lack of industry information. The potential size of PFC emissions from these industries will be further discussed in Section 5.2 when comparing the available AL industry BU emissions in China to those derived from TD methods.

PFC emissions from Taiwan's SC industry are certain to exist, but we were unable to access the data necessary to derive BU estimates. PFC emissions from North Korea are likely to be negligible given our understanding of the industries responsible for their emissions.

4. Model Prior Emission Distributions and Magnitudes Used for the Inverse Modeling of Regional Emissions of CF_4 and C_2F_6 in East Asia

The spatial distribution, quantity, and uncertainties of the prior flux field can influence the posterior emissions estimate from Bayesian inversion frameworks. For example, if the prior emission uncertainty is too small, and the observation uncertainty too large, then the inversion will be too strongly tied to the prior emissions. In addition, a prior for CF_4 and C_2F_6 based on the best available BU information (see Section 3) is still likely to be highly uncertain, as past studies of PFC emissions from China have shown TD emissions derived from observations that were substantially larger than the reported BU estimates (Arnold et al., 2018; Kim et al., 2010; Li et al., 2011; Saito et al., 2010). Also changes in global TD emissions (Say et al., 2021) suggest that regional emissions in East Asia are likely to have changed significantly over time. Therefore, we use an ensemble of nine inversions with a range of prior emissions, which were produced by combining three different prior flux distributions with three different total prior emission magnitudes with corresponding uncertainties.

Our prior distributions are based on the best information available as of 2010 (see Section 4.1), while our magnitudes start from the mean of the BU emissions for 2008–2010, the initial 3 years in our study period, and further adjusted as explained in Section 4.2. We keep the nine emission magnitudes and distribution combinations constant for all years (2008–2019). This ensures that the year-to-year trends in the posterior results are not biased by a change in the priors and are more likely driven by observations. Of note, the range of emission magnitudes and uncertainties were determined by repeated inversions, and examining the convergence of the posterior emissions starting from different prior estimates, as will be further discussed in the following sections.

4.1. Prior Distributions

The first examined prior distribution is based on 2010 global population (CIESIN et al., 2005). This is not realistic given our understanding that industrial PFC emission sources are localized, but does have the benefit of reducing prior emissions in many of the unlikely regions with low population, for example, the Tibetan Plateau in China. Population distribution has often been used as a reasonable first approximation when more specific information is not available (Fang, Park, et al., 2019; Fang, Yao, et al., 2019; Stohl et al., 2010).

Our second prior distribution adjusts the population prior distribution by flattening the emissions (i.e., all grids are assigned uniform prior emission fluxes) for regions in the model domain with high sensitivity, namely the Chinese provinces of Anhui, Beijing, Hebei, Jiangsu, Liaoning, Shandong, Shanghai, Tianjin and Zhejiang, referred to as "eastern China," the Korean Peninsula, and the regions of Chūgoku, Kansai, Kyūshū,Okinawa, and Shikoku in Japan, referred to as "western Japan" (Park et al., 2021; Rigby et al., 2019). Flattened priors can be unbiased in terms of emission locations, such that the distribution of emissions in the posterior could point to likely emission hot spots, but such inference is reasonable only in regions where the influence on the observations is relatively strong. Also, for China, uniformly distributing the country total emissions led to problematic biases in the prior distribution, for example, assigning significant emissions in western regions with low transport sensitivity where we do not expect any emissions, while also leading to significantly lower prior emissions in eastern China compared to the other distributions as emissions are evenly spread to other regions of the country. As such, we chose to flatten the prior only in the high sensitivity regions where such an approach can potentially add meaningful information through the inversion (Figure 1), while leaving the low sensitivity regions with the population density distribution.

Our third prior distribution is a specific point source distribution based on likely locations of PFC emission sources. We identified approximate locations of 127 AL smelters in China (web-based search in 2011), then identified exact coordinates through Google Earth™, which was possible due to the distinct physical structure of AL smelters (e.g., multiple smelter lines can be seen at 36°53′17.84″N, 101°43′25.46″E (Qinghai Aluminum) with their distinct elongated buildings (hundreds of meters to 1 km) and flu gas collecting and treatment systems). We found information on 2011 manufacturing capacities for 106 smelters, while the mean of these known production capacities were assigned to the other 21 smelters. These manufacturing capacities provided the basis for disaggregating AL industry total emissions to each AL smelter location. The location of SC foundries in China, Japan, Korea, and Taiwan were adopted from Mühle et al. (2019,

also web-search based). As information on SC production capacities were not readily available, all locations were presumed to have equal emission strengths. This point source distribution, while potentially the most realistic, can also be problematic in the inversion due to inaccuracies in the prior information. This is especially true for our case of keeping the prior distribution constant for all years, as we potentially add bias by not accounting for changes in specific industry source locations and/or strengths changing over time. To ensure that the inversion model can deal with these uncertainties based on the information in the observations, we apply 10% of the total country-specific emissions as a "base" prior distribution based on population density, ensuring that some minimum prior emissions are applied to all grids.

Prior distributions beyond our model domain are not expected to influence our results, but to ensure that these distributions are not completely unrealistic, we apply a population density distribution for these regions.

The resulting three prior distributions are shown in Figure C1.

4.2. Prior Magnitudes

Our prior magnitudes for Japan and Korea are based on the BU emission estimates before abatement for SC and FPD industries from their NIRs (Section 3.2), assuming that these estimates represent a theoretical upper limit of emissions. The "base" emission magnitudes are derived from the mean of 2008–2010, while two others are half of (×0.5, "low") and twice (×2, "high") the base emissions. Uncertainties are 30% (base), 15% (high), and 45% (low), respectively, resulting in identical absolute uncertainties for the base and high magnitude priors and slightly smaller absolute uncertainties for the low magnitude prior. The uncertainty for the low magnitude prior was adjusted based on preliminary inversion tests showing that the combination of small prior magnitude and high absolute uncertainty introduced instabilities in the inversion results.

For China, we begin with separate emission estimates for AL and SC/FPD industries. Our Chinese AL industry emission estimates are detailed in Section 3.1, and our priors use the mean of the 2008–2010 emissions. For China's SC/FPD emissions, our study lacked access to the relevant industry activity data, so we use the ratio of installed SC production capacity between China and Korea, reported to be 0.53 as of July 2011 (IC Insights, 2011) multiplied by the base emission magnitudes for Korea as detailed above. Preliminary inversion tests, as well as top-down results from previous studies (Arnold et al., 2018; Kim et al., 2010; Li et al., 2011; Saito et al., 2010) showed that the total prior emissions derived this way for China are significantly lower than the expected emissions. As such, we derive prior emissions that are ×1.5 ("low"), ×2.5 ("base"), and ×3.5 ("high") for CF_4 and ×3 ("low"), ×4.5 ("base"), and ×6 ("high") for C_2F_6 of the mean 2008–2010 emissions, chosen such that the high prior magnitude approximately matches the highest posterior emissions in our results, while relatively lower priors are also tested to ensure that the inversion is not biased by the high prior magnitudes. We assign high uncertainties to these prior magnitudes, 100%, 60%, and 50% for the low, base, and high priors, respectively, such that the absolute uncertainties are approximately matched among the different prior magnitudes, and the the magnitude of the prior uncertainty (3.72 Gg CF_4, 0.796 Gg C_2F_6) is closely aligned to the magnitude range of the prior magnitudes (4.96 Gg CF_4, 0.796 Gg C_2F_6).

For Taiwan, where direct reporting of BU emissions is not available, we take the ratio of Taiwan's installed production capacity to those of Korea, reported to be 1.25 as of July 2011 (IC Insights, 2011) and multiplied it by the priors derived for Korea, assuming that all emissions will be from SC/FPC industries. For North Korea, where we do not expect any significant PFC emissions, we apply 10% of the emissions assigned in Korea (South) as a default value, but do not discuss the results.

Emissions in regions not specified above are not expected to make a detectable impact on our results, either due to lack of sensitivity in our observations or being outside the model domain, but to ensure the priors emissions in these regions are not unrealistic, we assign the remaining quantities of the mean global TD total emissions for 2008–2010 after removing the emissions we apply to East Asia. In addition, no emissions are assigned to ocean grids, as PFC emissions from the oceans are highly unlikely to influence our results.

The resulting base, high, and low prior magnitudes and uncertainties derived for China, Japan, Korea, and Taiwan are shown in Table C1.

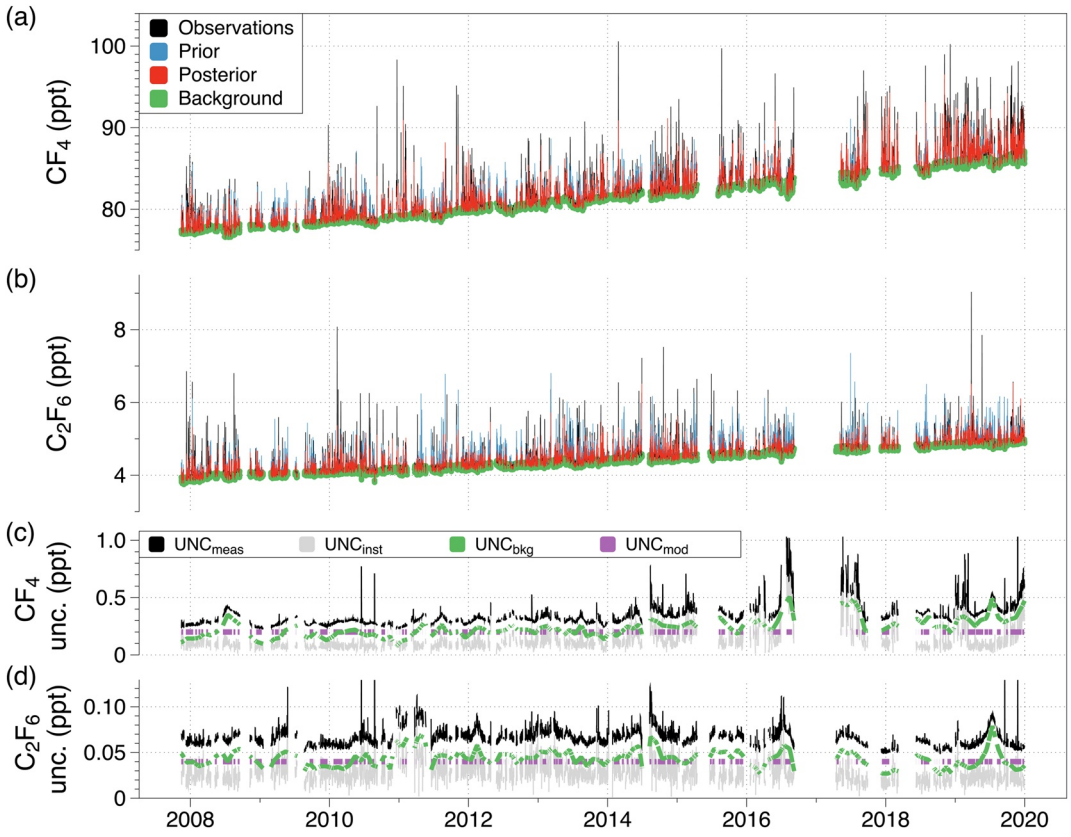

Figure 3. Time series of *in situ* observations of (a) CF_4 and (b) C_2F_6 at Gosan (black). Also shown are statistically determined background (green) and modeled concentrations based on convolution with transport and prior (blue) or posterior (red) emissions in the FLEXINVERT+ inverse modeling scheme. The prior used for these modeled concentrations is the flattened distribution at base magnitudes, see Section 4.3 for details. Shown below is the total measurement uncertainty (UNC_{meas}, in black) assigned for these observations, as well as the components that define it, namely the instrumental uncertainty (UNC_{inst}, in gray), the background uncertainty (UNC_{bkg}, in green), and the model representation uncertainty (UNC_{mod}, in purple), plotted over time for (c) CF_4 and (d) C_2F_6. See discussions in Sections 4.1 and 4.2 for details regarding the specific definitions of these uncertainties.

5. Top-Down Inverse Modeling of Regional Emissions of CF_4 and C_2F_6 in East Asia

5.1. In-Situ Observations at Gosan (Jeju Island, Korea)

Atmospheric concentrations of CF_4 and C_2F_6, shown in Figure 3, are measured *in-situ* at Gosan (126.16°E, 33.29°N, 17 m above ground, 89 m above sea level: Figure 1) with a "Medusa" gas chromatograph mass spectrometer (GC-MS) instrument (Arnold et al., 2012; Miller et al., 2008) as part of the AGAGE network. The measurements have a temporal frequency of approximately 2 h and are reported as dry air mole fractions on SIO-05 calibration scales (Prinn et al., 2018). Here we use measurements from November 2007 to December 2019. Analytical precisions are calculated daily based on the variability (standard deviation) of the working standard measured between each observation (10–11 measurements per day). While typical values are below 0.3% for CF_4 and below 1% for C_2F_6 of the observed atmospheric concentrations, they change significantly over time due to instrumental problems, as shown in Figure 3 (UNC_{inst}). These analytical precisions defined here contributed to the total measurement uncertainty assigned in our model, as further discussed in Section 5.2.

So-called "background" conditions, during which the mole fractions measured at Gosan are minimally influenced by emissions in East Asia, were derived using a statistical approach developed within AGAGE, which uses a 121-day moving window to identify positive outliers from a Gaussian distribution that represent pollution events (O'Doherty et al., 2001). "Enhancement" concentrations over background, used in

the model framework, were calculated by first binning the concentrations during background conditions by month, then linearly extrapolating between the monthly mean background concentrations (assumed to represent the fifteenth of each month) to derive background concentrations at each measurement time, and subtracting these extrapolated background concentrations from the corresponding measured concentrations. The uncertainty of our background is defined as the variability (standard deviation) of the concentrations in the monthly binned background, and linearly extrapolated from month to month similarly to the background concentrations. Note that our background uncertainty typically increases during summer when southern transport tends to increase the background concentration variability (Figure 3, UNC_{bkg}; Li et al., 2018). This background uncertainty defined here contributes to the total measurement uncertainty used in our model, as further discussed in Section 5.2.

Many of the gaps in the measurement data occurred in summer and early autumn, when operations were interrupted due to typhoons and heavy rains. One significant gap from October 2016 to April 2017 is due to extensive damage from typhoon Chiba. These data gaps impact the performance metrics of our model results, as further discussed in Section 5.3.

5.2. Inverse Model Approach

FLEXINVERT+ is a Bayesian inversion framework for estimating surface-atmosphere fluxes of various trace gases combining atmospheric measurements of trace gas mole fractions, modeling of air transport from sources to the measurement location within the model domain, and a prior flux field with predefined uncertainties. The model minimizes the following cost function (Thompson & Stohl, 2014):

$$J(p) = 1/2 \times (p - p_0)^T \mathrm{B}^{-1} (p - p_0) + 1/2 \times (H(p) - y)^T \mathrm{R}^{-1} (H(p) - y) \quad (5)$$

where p is the state vector, p_0 is its prior estimate, y is the measured enhancements over "background" (i.e., mole fractions in the air entering the model domain), **B** is the prior error covariance matrix, H is the atmospheric transport function (chemical removal of the PFCs during transport is negligible), and **R** is the measurement error covariance matrix. See Thompson and Stohl (2014) for further details.

We use the temporal resolution of the measured enhancements (approximately 2-hourly) and all hours of the day, with no temporal averaging for the inversion. The assigned total uncertainty for each enhancement (UNC_{meas}) is calculated as the quadratic sum of three terms:

$$\mathrm{UNC}_{\mathrm{meas}} = \sqrt{(\mathrm{UNC}_{\mathrm{inst}})^2 + (\mathrm{UNC}_{\mathrm{bkg}})^2 + (\mathrm{UNC}_{\mathrm{mod}})^2} \quad (6)$$

where UNC_{inst} refers to the instrumental analytical uncertainty, based on repeated measurements of the working tank, and UNC_{bkg} refers to the uncertainty of our background estimates, based on the monthly standard deviations observed in our background observations (see Section 5.1 for details). UNC_{mod} refers to any additional model representation uncertainty associated with the model representation of this measurement (i.e., due to the finite resolution and atmospheric transport errors), which is difficult to estimate directly. As such, we assume an arbitrary value of 0.2 ppt for CF_4 and 0.04 ppt for C_2F_6, which are approximately equal to the mean UNC_{bkg} values for 2008–2019. The timeseries for UNC_{meas}, UNC_{inst}, UNC_{bkg}, UNC_{mod} for CF_4 and C_2F_6 are presented in Figures 3c and 3d, respectively. One feature of UNC_{meas} is significant seasonal variability, driven by the increase in UNC_{bkg} over the summer months, where southern transport generally increases the variability of our background values (Li et al., 2018). Another significant feature is a general increase in UNC_{meas} for CF_4 after 2014, driven by an increase in UNC_{inst} for CF_4, reflecting instrumental problems.

Air transport to Gosan is estimated using the FLEXPART Lagrangian particle dispersion model version 10.4 (Pisso et al., 2019), driven by global meteorology from the National Centers for Environmental Prediction's Climate Forecast System Reanalysis model at 0.5° × 0.5° spatial and 1-hourly temporal resolution (Saha et al., 2010, 2011). In FLEXPART, 50,000 virtual particles were released during a 30-min window centered around each measurement time and tracked backwards in time for 20 days. Footprint sensitivities (i.e., how sensitive the measurements at Gosan are to emissions from each 0.5° × 0.5° grid in the modeling domain) are estimated from the lower 100 m of the model output (Stohl et al., 2010).

Our inverse modeling domain covers the wider East Asian region, including all of China (70°–155°E, 10°–55°N). The inverse calculation of emissions is carried out over a variable sized grid (Figure C2), aggregating the base grids at a resolution of 0.5° × 0.5° to larger grid sizes with decreasing sensitivity. By default, the final exported posterior disaggregates these larger grids back to the base grid resolution based on prior distribution. All ocean grids are ignored assuming negligible PFC emissions. The inverse calculations are performed independently for each calendar year from January to December, and no multi-year smoothing is applied to the results, thus keeping each annual inversion result independent. We assume that our approach of deriving baseline from observations (see Section 5.1) is an acceptable approximation of the PFC concentrations in air entering the model domain, and that it would sufficiently account for the atmospheric variability and trends outside of our model's spatial and temporal domain. We assume a spatial error correlation length of 200 km in our priors, while temporal error correlations were not considered.

We employ a number of diagnostics for each annual inversion model run to analyze the performance. The reduced chi-square for each inversion run is equal to half the value of the cost function divided by the number of observations and is an approximate measure for the appropriateness of the uncertainties, which when well-chosen should result in a reduced chi-square value close to 1. The information content of the observations was also calculated for each inversion run. It is a measure of the factor by which uncertainty decreases as more observations are added, a generalization of the scalar concept of signal-to-noise ratio (Rodgers, 2000), and calculated using the following formula:

$$\text{Information content} = 0.5 \times \ln\left(\left|\mathbf{B} \cdot \mathbf{A}^{-1}\right|\right) \tag{7}$$

where **B** refers to the prior error covariance matrix, and **A** refers to the posterior error covariance matrix.

Other diagnostics are calculated at the regional scale. Error reduction is calculated for each region as:

$$\text{Error Reduction}\left(\%\right) = 1 - \frac{\sum \sigma_{\text{post}}}{\sum \sigma_{\text{prior}}} \tag{8}$$

where σ is the uncertainty of each grid cell within the region, and presented as a percentage. The posterior convergence for each region is calculated as the ratio of the range of posterior magnitudes to the range of prior magnitudes (see Section 4 for details on the nine priors used in each annual inversion run), such that a quantity closer to zero represents better convergence, and presented in percent units. Relative posterior uncertainty is the ratio of the range of posterior magnitudes against the mean posterior value, and also presented in percent units. We also calculate the annual minimum, maximum, and standard deviations of the nine posterior magnitudes per region.

5.3. Modeled Regional Emissions Results

Here we focus on the results and diagnostics of the model posterior for the full model domain in East Asia. In Section 6, we will discuss how we derive robust national emissions for individual countries from our East Asian posterior.

Overall, our results over East Asia, shown in Figure 4 (see Table C2 for details), suggest that the inverse model produces robust posteriors from the range of priors applied over this domain. We find significant error reductions within East Asia of 32% for CF_4 and 31% for C_2F_6 (mean over 2008–2019) while our East Asian posterior converge to within 16% of the prior range for CF_4, and 12% for C_2F_6 (mean over 2008–2019). The uncertainties we report for the posterior emissions is the range of minimum and maximum among the nine annual posterior emissions (based on the nine priors used each year, see Section 4 for details), and we find that this range is equal to 16% of the posterior emissions for CF_4, 14% for C_2F_6, when assessed over 2008–2019 (see relative uncertainty in Figure 4). The Taylor diagrams illustrating our strong posterior convergence is presented in Figure C3. The reduced chi-square values calculated for each year, shown in Figure 4 for CF_4 and C_2F_6, range from 0.7–3.5, suggesting that our definitions of the prior (detailed in Section 4) and measurement uncertainties (detailed in Sections 5.1 and 5.2) are generally sound. Refer to Section 5.2 for specific definitions of the diagnostics discussed above.

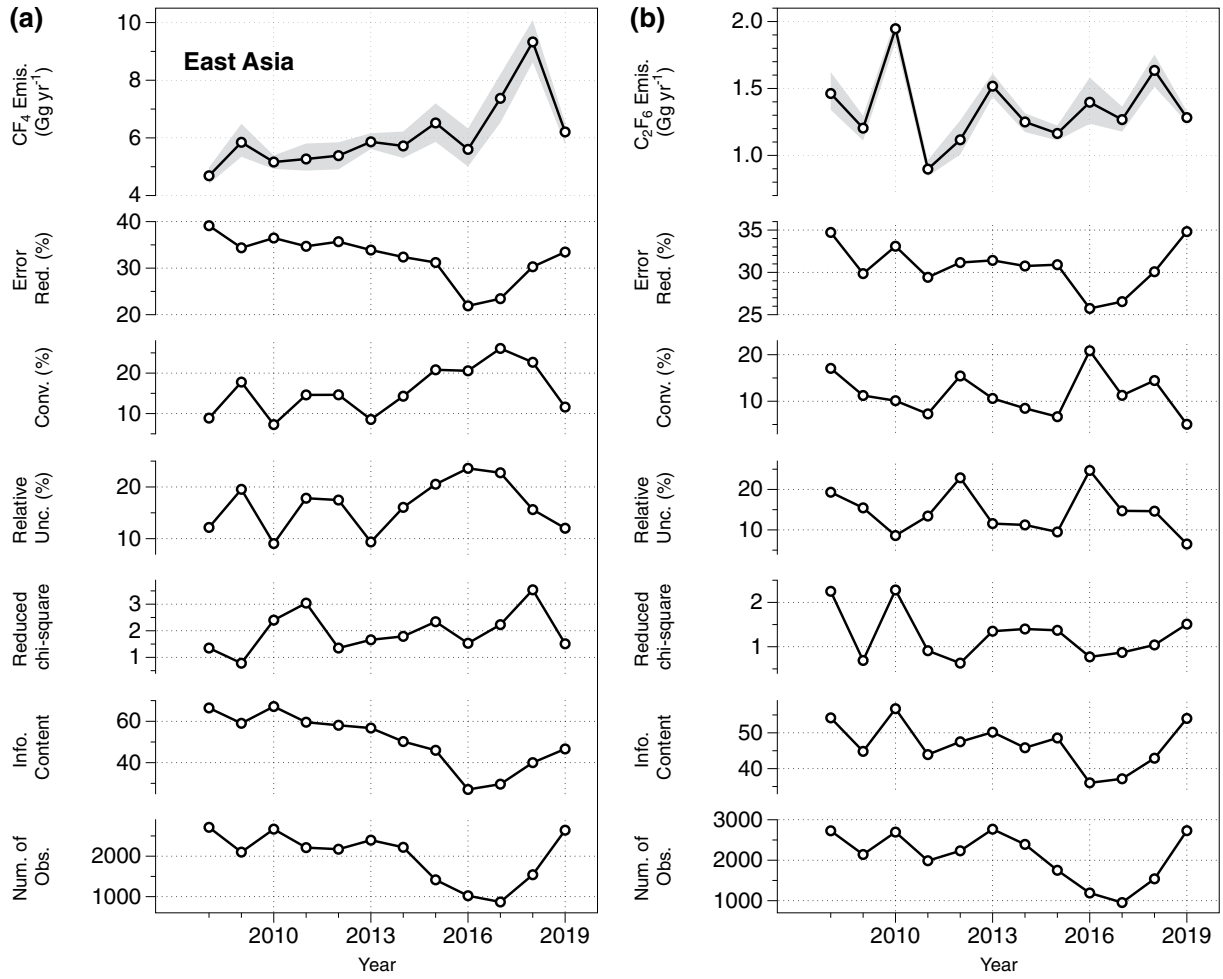

Figure 4. Top-down annual emissions of (a) CF_4 and (b) C_2F_6 estimated for the East Asian domain (China, Japan, Korea, and Taiwan) during 2008–2019 using the FLEXINVERT+ inversion framework, with associated model diagnostics plotted for posterior error reduction, posterior convergence, relative uncertainty, reduced chi-square value, information content value, and the number of observations used in the annual inversions. Refer to text in Section 5.2 for detailed descriptions of these diagnostics, and Section 5.3 for discussions of these results.

To show how the different spatial distributions test our inverse model framework, we compare the annual East Asian posterior emissions by prior distribution in Figure 5. When aggregated over East Asia, we find that the convergence for a given prior distribution (i.e., posterior convergence in varying the prior and prior error magnitudes within the same prior distribution) can be better than convergence between different prior distributions, with the point source prior distribution resulting in higher posterior for some years. As such, our results suggest that the prior distribution is an important driver of uncertainty in our inversion framework, as the spatial locations of the emissions are difficult to fully resolve within the model, especially in our case of using only one observation site, and emphasize the importance of testing different prior distributions to better assess the systematic uncertainties in the posterior results.

These uncertainties from prior distributions are to be expected given that our study is based on one observation site, and the spatial distribution of the posterior emissions still carries substantial uncertainties. For this reason, we focus our analysis on the large scale, that is, the annual totals at regional scales, and do not focus on the finer spatial patterns in the posterior results. The uncertainties at large scales are smaller than at finer scales owing to the negative correlations between grid cells in the posterior covariance matrix, where these negative correlations indicate where two grid cells cannot be independently resolved.

The one limited case where we may have some meaningful information is in the case of our flattened prior, where we apply an unbiased flat prior distribution in the grids with relatively high sensitivity to Gosan (see

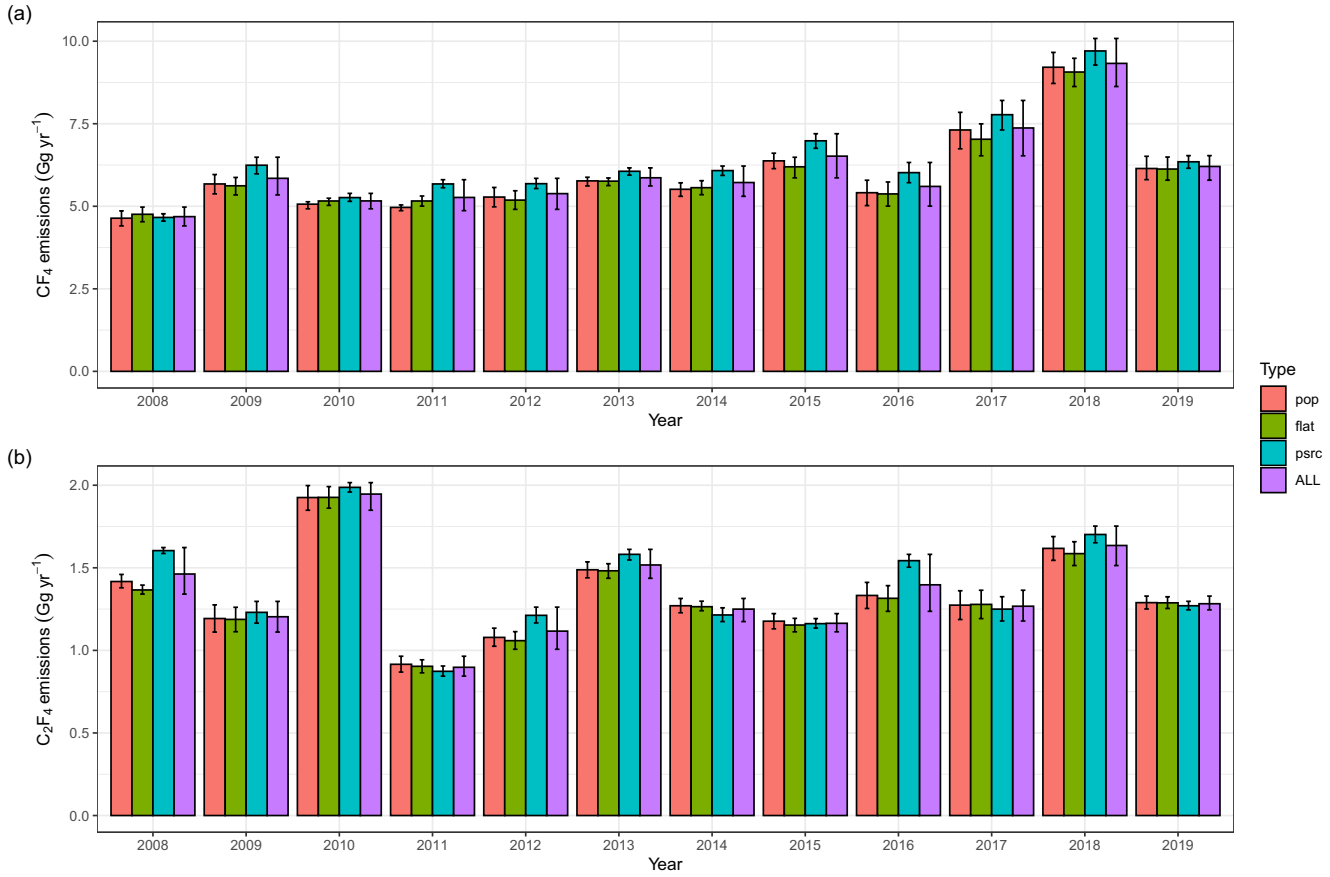

Figure 5. Annual posterior results for (a) CF_4 and (b) C_2F_6 by prior distribution type, namely population ("pop," in red), flattened ("flat," in green), and point source ("psrc," in blue), as well as for all nine runs combined ("ALL," in purple). The error bars represent the minimum and maximum values of the three model runs (base, high, low prior magnitudes in case) performed for each prior distribution or the nine model runs for a particular year.

Section 4.1 for details). Our results shown in Figure 6 suggest that the hotspot locations in eastern China and Korea for CF_4 may have shifted significantly over time, while the C_2F_6 source locations remain more or less the same. We also note that for the non-flattened grids, the spatial distribution in our posterior largely follows the prior distribution by design, especially in the grids that are less sensitive to Gosan (as discussed in Section 5.2), and so our posterior distribution outside the flattened region should not be interpreted as resolved through the inverse model. Spatial plots of the other prior and posterior distributions are presented in, Figures C4 (CF_4) and C5 (C_2F_6).

One general feature of our results is year-to-year variability in the posterior emissions and also the various model diagnostics. While each of our annual posteriors are derived independent of each other, we also note significant differences in how each of the annual inversion model runs are constrained, as shown in the model diagnostics in Figure 4. As such, it's difficult to determine to what extent these year-to-year variabilities are driven by actual emission changes as opposed to increased model uncertainties due to weaker constraint. Generally, we see that the broad trends in our model diagnostics follow the number of observations used in each annual inversion. However, model performance will also be strongly influenced by the seasonal coverage of those observations and the year-to-year variability in transport patterns, for example, the frequency of southern transport events in summer (Li et al., 2018), and these nuanced differences may be better captured in the information content value (see Section 5.2 for definition).

Comparing our results between CF_4 and C_2F_6, we note that the year-to-year variability in their emissions do not seem correlated, and that the results for C_2F_6 have generally larger year-to-year variability and smaller information content values, likely due to the fact that the smaller emission magnitudes and observed concentrations for C_2F_6 significantly reduce our model performance for this species. Also of note is 2016, where

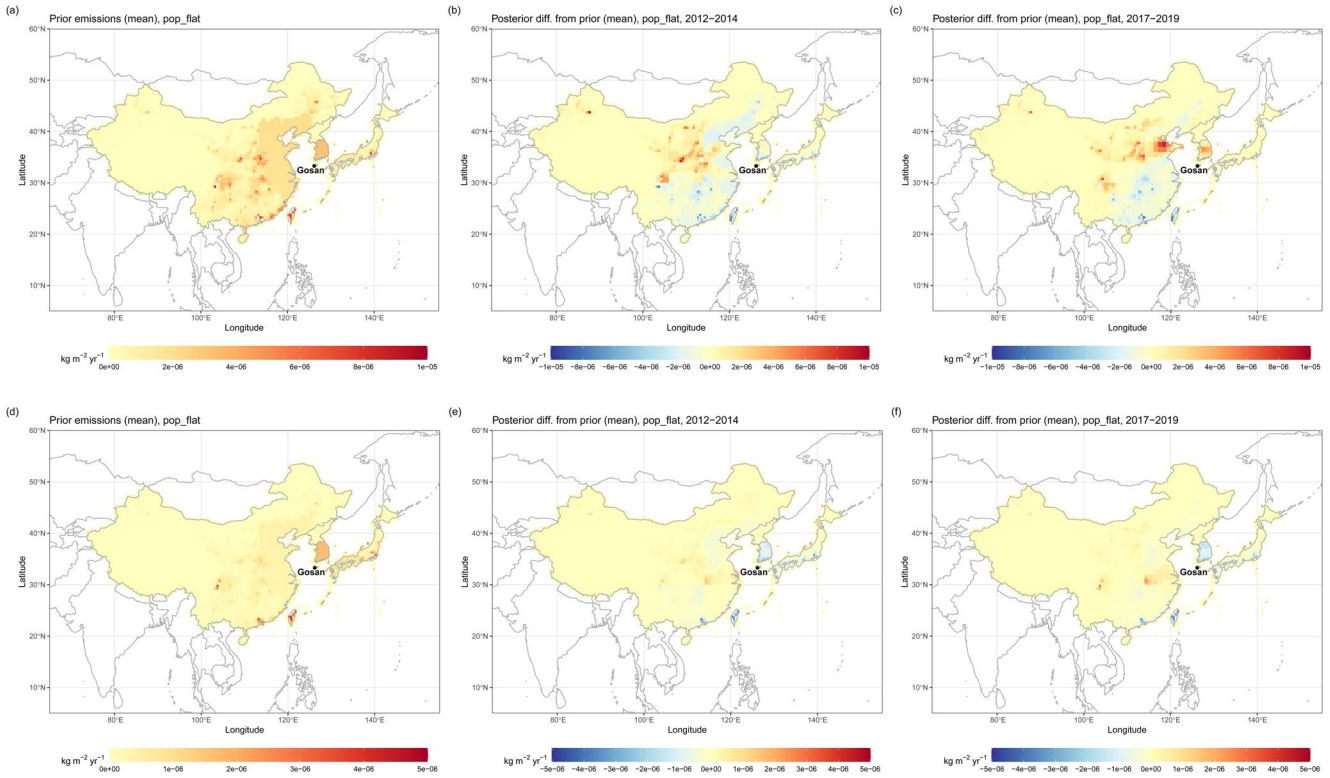

Figure 6. Spatial map of the flattened prior distribution for (a) CF_4 and (d) C_2F_6, with the mean posterior emissions derived in FLEXINVERT+ for 2012–2014 of (b and d) and 2017–2019 (c and f) for CF_4 and C_2F_6, respectively, plotted as difference from the prior. Plots for other prior distributions, as well as the standard deviations per each grid for 2017–2019 are available in supporting information (Figures C3 and C4).

the information content value is at minimum, and discussions presented later in Section 7 will show that the posterior emissions derived for CF_4 are somewhat low compared to adjacent years when viewed in context of other emissions data. While the information content value provides a qualitative metric for why the 2016 posterior may be more uncertain, it is difficult to identify the exact set of model constraints that led to the posterior being particularly low for this specific year.

To test our ability to identify emission changes at annual scales, we performed a set of model inversions where the annual division were shifted to November, allowing the inversion to target Chinese emission reductions during the financial crisis over November 2008 to March 2009. This alternate model configuration derives emissions in China for November 2008–October 2009 that are 51% lower than the mean emissions in November 2007–October 2008 and November 2009–October 2010, and significantly different from the results of the annual runs on calendar year divisions (Figure C6). This suggests that our inversion framework may be capable of identifying year-to-year differences in emissions under specific conditions, but further analysis into quantifying temporal uncertainties were beyond the scope of this work. Also, detecting emission changes at sub-annual scales is likely to be difficult given the seasonality of wind advection to Gosan.

6. Estimating Top-Down National Emissions From Inverse Modeling

Here we disaggregate the inverse model posterior results along the borders of China, Japan, Korea, and Taiwan, to compare them to reported national bottom-up emissions (see Section 7 for details). This disaggregation occurs during the post processing of the inverse model posterior and requires further analysis on the added uncertainties at these reduced spatial domains and the influence of diminishing sensitivities for regions far away from the measurement site. The national emissions derived are shown in Figure 7.

For China, while we find significant error reductions (32% for CF_4, 27% for C_2F_6, mean over 2008–2019) and posterior convergence (17% for CF_4 and C_2F_6, mean over 2008–2019), the model performance is also

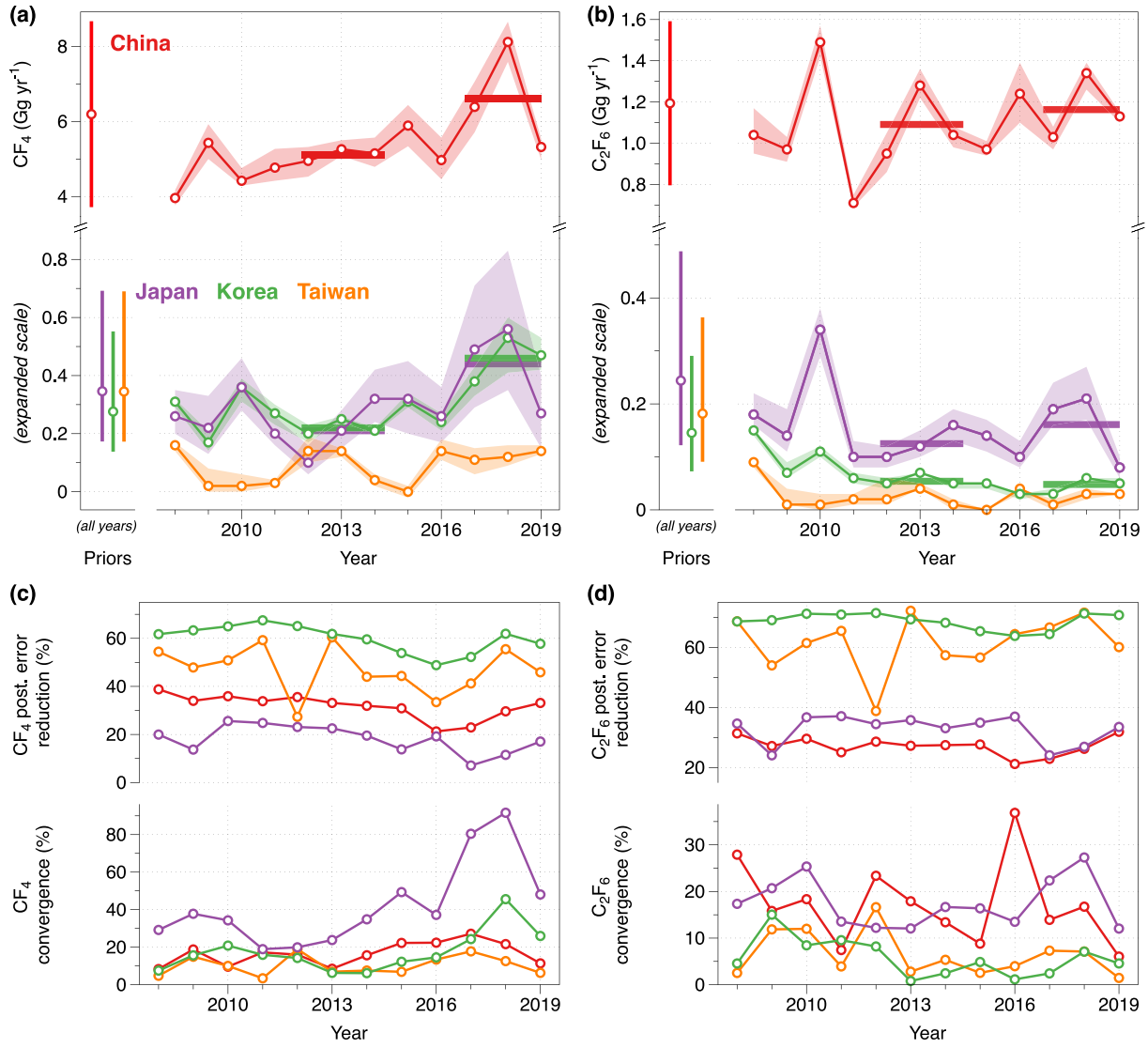

Figure 7. Top-down annual emissions of (a) CF_4 and (b) C_2F_6 estimated for China (red), Korea (green), Japan (purple), and Taiwan (orange) during 2008–2019 using the FLEXINVERT+ inversion framework, with associated model diagnostics plotted for (c) CF_4 and (d) C_2F_6, namely posterior error reduction, and posterior convergence (see text in Section 5.2 for detailed descriptions and discussions of these diagnostics). The bars shown for the priors in (a and b) show the three prior magnitudes ("low," "base," and high") tested in this study (see Section 4 for details), and the uncertainty plotted on the posterior emissions are the range of results from the 9-member inversion ensemble. The solid horizontal lines in the graph highlight the mean emissions for the periods of 2012–2014 and 2017–2019 for each region, respectively. Note that Taiwan's emissions show strong bimodality, therefore our study takes the mean emissions from 2008, 2012–2013, and 2016–2019 as the mean emissions for Taiwan during 2008–2019. See discussions in Section 6 for details.

significantly worse in the western subregions less sensitive to Gosan. This point is illustrated in Figure 8, separating out eastern China (as defined in Rigby et al. (2019) and Park et al. (2021), and our priors described in Section 4.2) where the robust error reductions and convergence are close to those of Korea, and the rest of China where the model metrics are significantly worse. It is notable that much of the year-to-year variability in the total Chinese posterior emissions is driven by the variability in the rest of China, while emissions derived for eastern China are generally more stable year-to-year. An additional consideration is that the Tibetan Plateau makes up a large portion of western China to which Gosan observations are insensitive, and our inversion effectively ignores this region by prescribing negligible prior, following the low population density in this area (see Section 4.1 for details), and in how those priors are largely unchanged during the inverse model calculation.

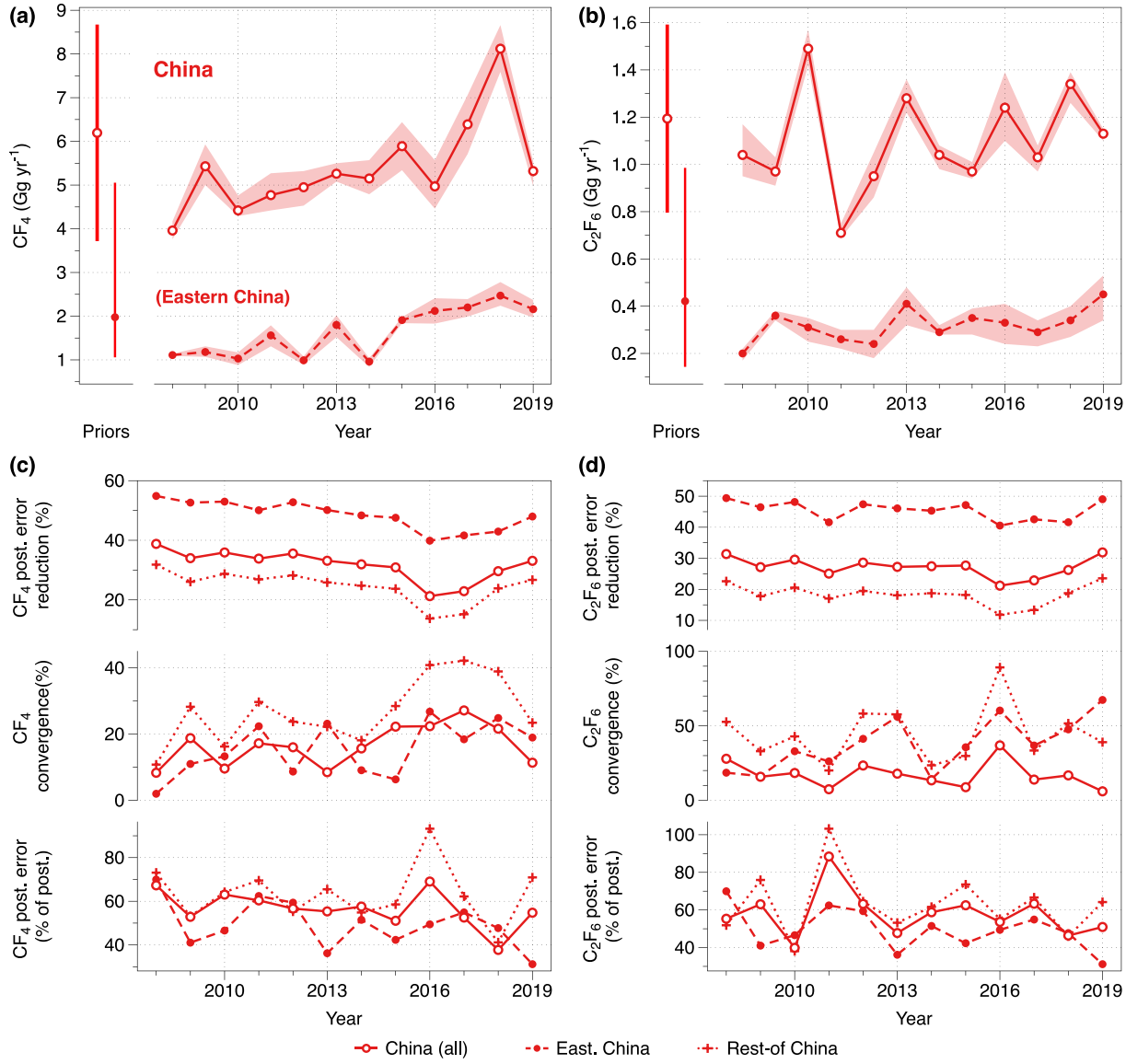

Figure 8. Comparison of model posterior emissions and diagnostics for China (in solid lines and open circles), eastern China (dashed lines in filled circles; see Section 4.1 for the geopolitical definition), and rest of China (in dotted lines and plus symbol). The bars shown for the priors in (a and b) show the three prior magnitudes ("low," "base," and high") tested in this study for China and eastern China (see Section 4 for details), and the uncertainty plotted on the posterior emissions are the range of results from the 9-member inversion ensemble. Refer to Section 5.2 for definitions of the model diagnostics, and see Section 6 for detailed discussions of these results.

For Japan, we find that posterior error reduction and convergence is generally lower than the other East Asian countries, with mean error reductions of 18% for CF_4 and 33% for C_2F_6, and mean convergence of 42% for CF_4 and 17% for C_2F_6 over 2008–2019. In addition, as with China, we find that model performance is significantly reduced in comparing the more sensitive western Japan (as defined in Rigby et al. (2019) and Park et al. (2021), and also in the priors described in Section 4.2) to the rest of Japan, as shown in Figure 9. We also find that significant year-to-year variabilities exist in western Japan that generally follow the variability patterns in rest of Japan, suggesting that the model constraint even in the more sensitive western Japan may be relatively poor.

For Korea (South), our results show robust constraint on the posterior emissions with the highest error reductions (60% for CF_4, 69% for C_2F_6, mean over 2008–2019) and best posterior convergence (17% for CF_4, 6% for C_2F_6, mean over 2008–2019) among the East Asian countries considered in this study. Model

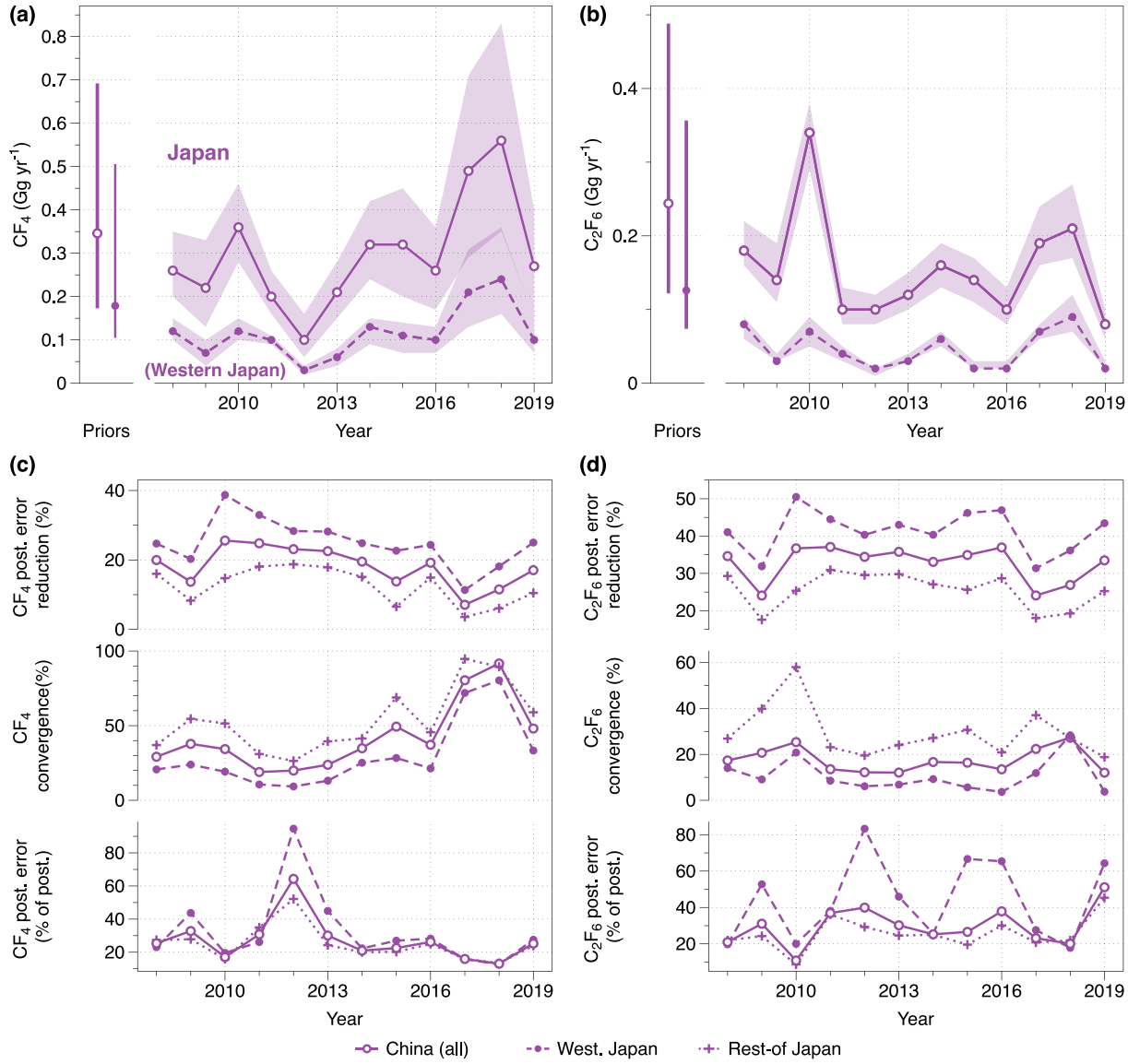

Figure 9. Comparison of model posterior emissions and diagnostics for Japan (in solid lines and open circles), western Japan (dashed lines in filled circles; see Section 4.1 for the geopolitical definition), and rest of Japan (in dotted lines and plus symbol). The bars shown for the priors in (a and b) show the three prior magnitudes ("low," "base," and high") tested in this study for Japan and western Japan (see Section 4 for details), and the uncertainty plotted on the posterior emissions are the range of results from the 9-member inversion ensemble. Refer to Section 5.2 for definitions of the model diagnostics, and see Section 6 for detailed discussions of these results.

performance is similarly robust for both CF_4 and C_2F_6, and these results are to be expected given its relatively close proximity to Gosan.

Given the increased spatial and year-to-year uncertainties discussed above, we conclude that our discussions of national emissions in China, Japan, and Korea should be limited to those after multi-year averaging and in analyzing long-term trends, where the effects of the underconstrained spatial uncertainties that lead to the year-to-year variabilities can be substantially reduced. Specifically, we focus our discussions in Section 7 on broad changes in total emissions between 2012–2014 and 2017–2019, or on long-term trends during 2008–2019, over spatial scales of East Asia or for China, Japan, and Korea, and do not discuss any of the spatial patterns within the national borders.

For Taiwan, we find that despite relatively robust model metrics, with posterior error reductions of 47% for CF_4 and 61% for C_2F_6 over 2008–2019, the posterior emissions are strongly bimodal, such that some years

Table 1
Comparison of Top-Down Emissions for CF_4 and C_2F_6 Globally and in East Asia From 2012–2014 to 2017–2019. Full Results for All Years are Available Table C2

	CF4 (Gg yr^{-1})							C2F6 (Gg yr^{-1})						
Years	**Global**	**unc.**	China	Japan	Korea	**East Asia**	**unc.**	**Global**	**unc.**	China	Japan	Korea	**East Asia**	**unc.**
2012–2014	11.23	0.05	5.12	0.21	0.22	5.55	0.15	1.93	0.05	1.09	0.13	0.054	1.27	0.11
2017–2019	13.94	0.07	6.61	0.44	0.46	7.51	0.92	2.22	0.14	1.16	0.13	0.048	1.34	0.12
Diff.	2.71	0.09	1.49	0.23	0.24	1.96	0.93	0.29	0.15	0.07	0.00	0.007	0.07	0.16
(%)	*24*	*1*	*29*	*109*	*109*	*35*	*17*	*15*	*8*	*7*	*1*	*−12*	*5*	*13*

(2008, 2012–2013, and 2016–2019) show significantly higher emissions compared to the others. These bimodal patterns are likely driven by year-to-year variabilities in southern transport in the summer months, but identifying the specific model mechanisms that cause these bimodal patterns was beyond the scope of this work. As such, we report the mean of the years with significant posterior (2008, 2012–2013, and 2016–2019) to represent the mean emissions for Taiwan over 2008–2019, with uncertainties equal to the standard deviation of those years, and assume no significant trend in the emissions can be detected over this period.

Our nationally aggregated posterior results are in general agreement within the reported uncertainties of previous studies (Arnold et al., 2018; Kim et al., 2010; Li et al., 2011; Saito et al., 2010), as shown in Figure C7, although we note significant differences in how the uncertainties are defined for each study, and that the comparison is limited in scope, especially for C_2F_6. The full table of the inverse model results and diagnostics per region are presented in supporting information (Table C3), and a plot of the posterior results per country and subregion by prior distribution is available in Figure C8.

7. Discussion

7.1. Increases in Global PFC Emissions From 2012–2014 to 2017–2019

Our results for TD CF_4 emissions in East Asia (Table 1, Figure 10) identify an increase of 1.96 ± 0.93 Gg yr^{-1} in 2017–2019 compared to 2012–2014, a 35 ± 17% mean increase in emissions over this period. This is well matched with the increase in global emissions of 2.71 ± 0.09 Gg yr^{-1} from 2012–2014 to 2017–2019, suggesting that East Asian CF_4 emissions are likely a strong driver for the global increase in CF_4 emissions since 2012–2014. China is likely to be the largest contributor to this increase in terms of magnitude, but the largest percentage increase is found in Korea, where CF_4 emissions are shown to have doubled from 2012–2014 to 2017–2019.

For C_2F_6 emissions, our results for China, Japan, and Korea do not increase significantly from 2012–2014 to 2017–2019 (+0.07 ± 0.16 Gg yr^{-1}), and contrast the increase in mean global emissions (+0.29 ± 0.15 Gg yr^{-1} or 15 ± 8% yr^{-1}). The more or less stagnant C_2F_6 emissions for Japan and Korea are consistent with the reported phase out of C_2F_6 in their SC and FPD industries (GIO, 2020; GIR, 2020), and it seems less likely that emissions from these two countries would contribute significantly to an increase in global emissions. China's C_2F_6 emissions are calculated to have increased by 0.07 ± 0.14 Gg yr^{-1} from 2012–2014 to 2017–2019, equal to a 7 ± 12% increase over this period, but the statistical significance of this increase is difficult to assess given the large year-to-year variability in the posterior results for C_2F_6, which are more likely a reflection of systematic uncertainties in the inversion rather than changes in annual emissions. As such, our TD results are inconclusive in identifying East Asia's role in the global increase in C_2F_6 emissions from 2012–2014 to 2017–2019.

Overall, the TD East Asian emissions derived in this study (China, Japan, Korea, and Taiwan) are a dominant portion of the global TD emissions, equal to 52 (43–61)% and 67 (57–79)% over 2008–2019 and 55 (44–65)% and 64 (54–73)% over 2017–2019 for CF_4 and C_2F_6, respectively, taking into account the uncertainty range in both the global and East Asian TD totals. Our results emphasize the importance of accurately accounting for emissions in this region in understanding the global budgets of these compounds.

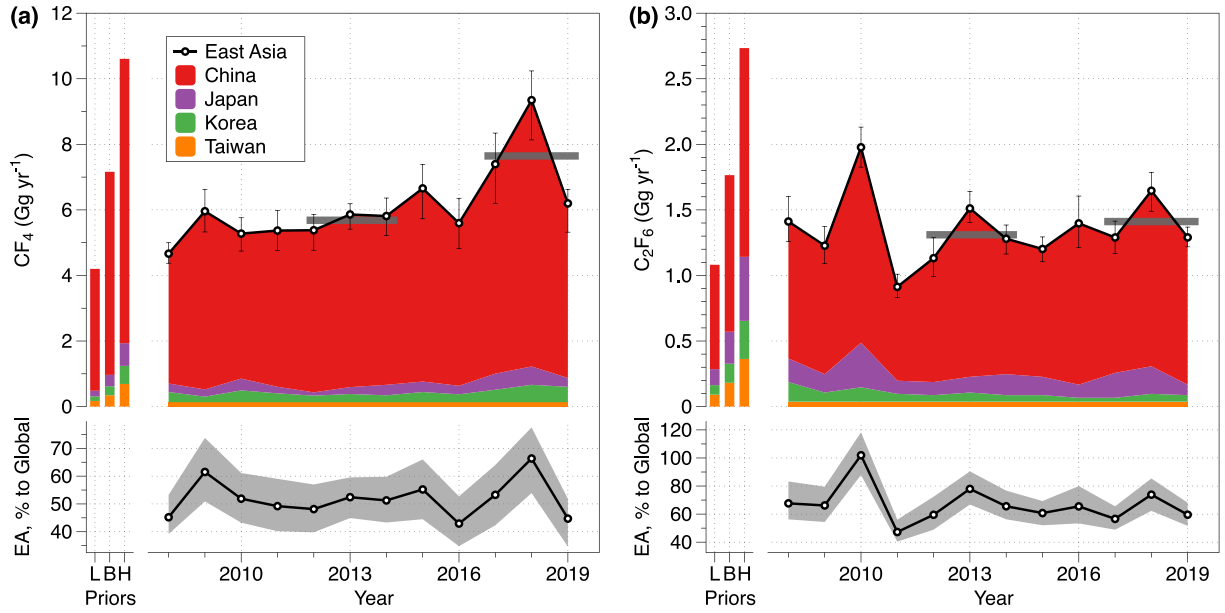

Figure 10. Top-down annual emissions of (a) CF_4 and (b) C_2F_6 estimated for East Asia during 2008–2019 using the FLEXINVERT+ inversion framework. The top plot shows the prior and posterior emissions for China (red), Japan (purple), Korea (green), and Taiwan (orange), while the bottom plot shows the total East Asian emissions as a percentage of the total global top-down emissions described in Section 2. The bars for the priors show the three prior magnitudes ("low," "base," and high") tested in this study. The uncertainty bars on the posterior emissions are the range of results from the 9-member inversion ensemble. The gray lines in the graph highlight the mean East Asian emissions for the periods of 2012–2014 and 2017–2019, respectively. Note that Taiwan's emissions are assumed to be constant, based on mean results from 2008, 2012–2013, and 2016–2019.

7.2. Trends in China's Top-Down and Bottom-Up Emission Estimates

The comparison of the long-term trends of China's TD PFC emissions and AL industry BU emissions (BU_{AL}) can help assess changes in emission characteristics from China's AL industry, and help infer the emission magnitudes of other sources for which reporting is limited, including China's RE, SC, and FPD sectors. Our analysis, presented in Figure 11 as 1-BU_{AL}/TD, suggests that the large discrepancy between the two estimates in the early years have been decreasing significantly over time. 1-BU_{AL}/TD for CF_4 is now approaching zero, which means agreement between TD and BU_{AL}, in recent years, while significant disagreement remains for C_2F_6 between the TD and BU_{AL} emissions, with 60% of the TD C_2F_6 emissions missing in the BU_{AL} C_2F_6 for 2017–2019. Despite these differences, our study finds that the TD versus BU_{AL} discrepancy in both CF_4 and C_2F_6 have decreased at a similar rate when comparing 2017–2019 to 2008–2010 (−3.5% and −2.2% per year on average for CF_4 and C_2F_6, respectively).

To further analyze industry-specific emissions in China, we performed a vector analysis of China's TD CF_4 and C_2F_6 emissions (Kim et al., 2014), using a combination of observed or reported C_2F_6/CF_4 emission ratios from China's AL and SC industries (see Text D1). Our results are significantly affected by uncertainties in our TD emissions and choice of industry emission ratios, but suggest that on average over 2008–2019, the AL industry is likely the dominant source of China's CF_4 emissions (76%), while China's C_2F_6 emissions are more skewed toward the SC industry (63%). Comparing 2017–2019 to 2012–2014, our results show that the AL industry emissions for both PFCs increased by 42% (1.6 Gg yr^{-1} CF_4, 0.15 Gg yr^{-1} C_2F_6) while the SC industry emissions remained nearly identical for CF_4 (3% decrease, −0.04 Gg yr^{-1}) and slightly decreased for C_2F_6 (11% decrease, −0.080 Gg yr^{-1}). This suggests that China's increase in PFC emissions over this period has been dominated by the AL (and potentially the RE) sector, which is in line with the significant increase in Chinese AL (and RE) production over the same period (Figure 11).

The overall decrease in discrepancy between China's TD and BU_{AL} PFC emissions could suggest that China's AL industry has significantly improved its PFC emissions-per-production ratio over time, and that the recently revised IPCC emission factors for China (Ottinger & Cai, 2019) used in this study closely match real-world conditions in recent years, but underestimate emissions for previous years. Our results of the

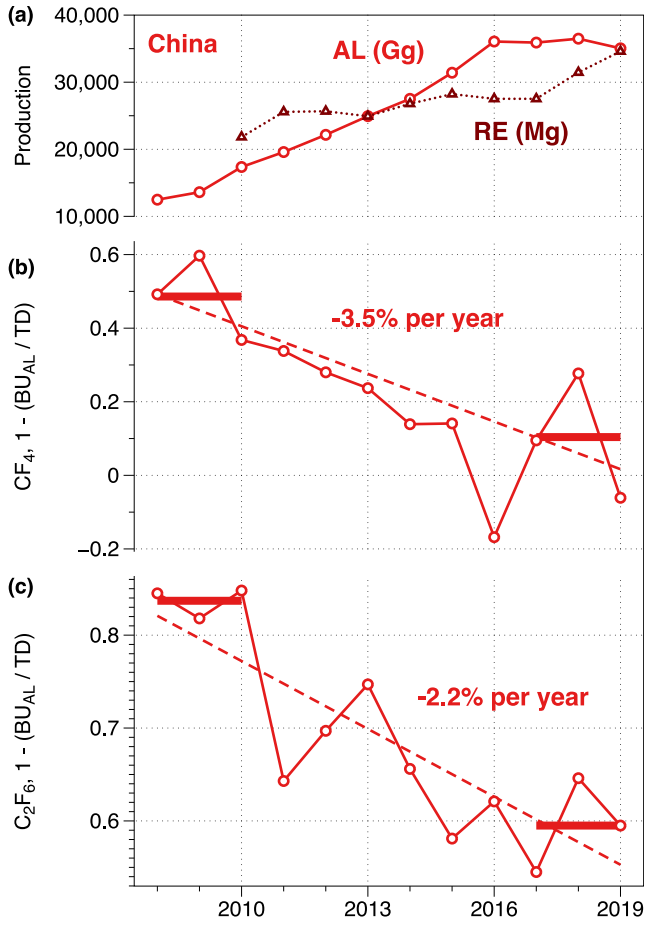

Figure 11. (a) China's aluminum (AL) and rare earths (RE) production compared to the discrepancy between China's top-down (TD) and AL industry bottom-up emissions (BU_{AL}) for (b) CF_4 and (c) C_2F_6. Ideal agreement is achieved when 1-(BU_{AL}/TD) equals zero. Note the unit differences in production for AL (Gg) and RE (Mg) industries.

CF_4 and C_2F_6 discrepancy reducing at a similar rate, and those from our vector analysis, are in line with this hypothesis. An alternate scenario could be that the observed decrease in the overall discrepancy is driven by emission reductions from other sources such as RE, SC, and/or FPD industries, but we lack industry reporting that could support this hypothesis. Further analysis into the changes in industry emission characteristics over time was deemed beyond the scope of this work, given the limited availability of relevant industry information.

Regarding the PFC emission magnitudes from China's RE, SC, and FPD industries, one interpretation of the good agreement in recent years between TD and BU_{AL} for CF_4 could be that CF_4 emissions from the other industries are relatively small, at least over the last few years. In addition, the source of the significant discrepancy found for C_2F_6 is not likely to be in the AL or RE industries given what is known about their emission ratios being skewed toward CF_4, which could suggest that China's SC and/or FPD industries consume and emit a significant amount of C_2F_6, which is in line with our results in the vector analysis of Chinese PFC emissions. Overall, our analysis finds clues to identifying the emission magnitudes of China's RE, SC, and FPD sectors, and a more thorough analysis could be a subject for future studies when more industry data is available.

7.3. Abatement Efficiencies in the Semiconductor Industry

Our study identifies significant differences between TD and NIR reported BU emissions in Japan and Korea, where SC and FPD industry emissions dominate total emissions (Figure 12). Here, we focus on the comparison of broad trends from 2012 to 2018 (based on NIR data availability).

For CF_4 in Japan, we find that the disagreement between TD and BU increases over time, in line with the increasing trend in consumption rather than the constant trend in the reported BU emissions after abatement. We find a similar disagreement in Korea, where the TD CF_4 emissions are found to step up in 2015, which is more in line with increased consumption over 2015–2018, and in disagreement with the reported BU emissions that suggest a significant step down in emission in 2015.

For C_2F_6, our results suggest that the TD versus BU disagreement in Japan may be increasing in time, while the two estimates for Korea are found to be broadly in agreement, although we note year-to-year variability. On average, Japan's TD is higher than the BU by 0.11 Gg yr^{-1} over 2012–2018, which is equal to ×3.6 of the reported BU emissions with abatement over this period.

Our findings of generally large TD versus BU discrepancies in CF_4 suggests that the uncertainties in the emissions of CF_4 are significant in the SC and FPD industries. Our results are in line with past studies finding that CF_4 is difficult to destroy in real world abatement conditions (Choi et al., 2012; Ou Yang et al., 2009), and the possibility of CF_4 being produced from the abatement of NF_3 (Czerniak et al., 2007; Ottinger & Cai, 2019). The results in Korea are especially striking, in that since 2015, where reporting suggests a significant decrease in emissions due to an increase in abatement, we find that TD emissions have actually increased for CF_4, but not for C_2F_6. Overall, our results suggest that abatement efficiencies are a significant uncertainty in the current BU calculations for the SC and FPD industries, especially for CF_4, and call for efforts to identify and apply abatement rates reflective of real-world conditions.

The gradual increase in Japan's TD versus BU discrepancy is a topic for further research, especially for C_2F_6 where the trend contradicts the gradual decrease in consumption over this period. One specific concern will be to account for emissions from other sources, such as fugitive emissions during PFC production, for which data availability is currently limited.

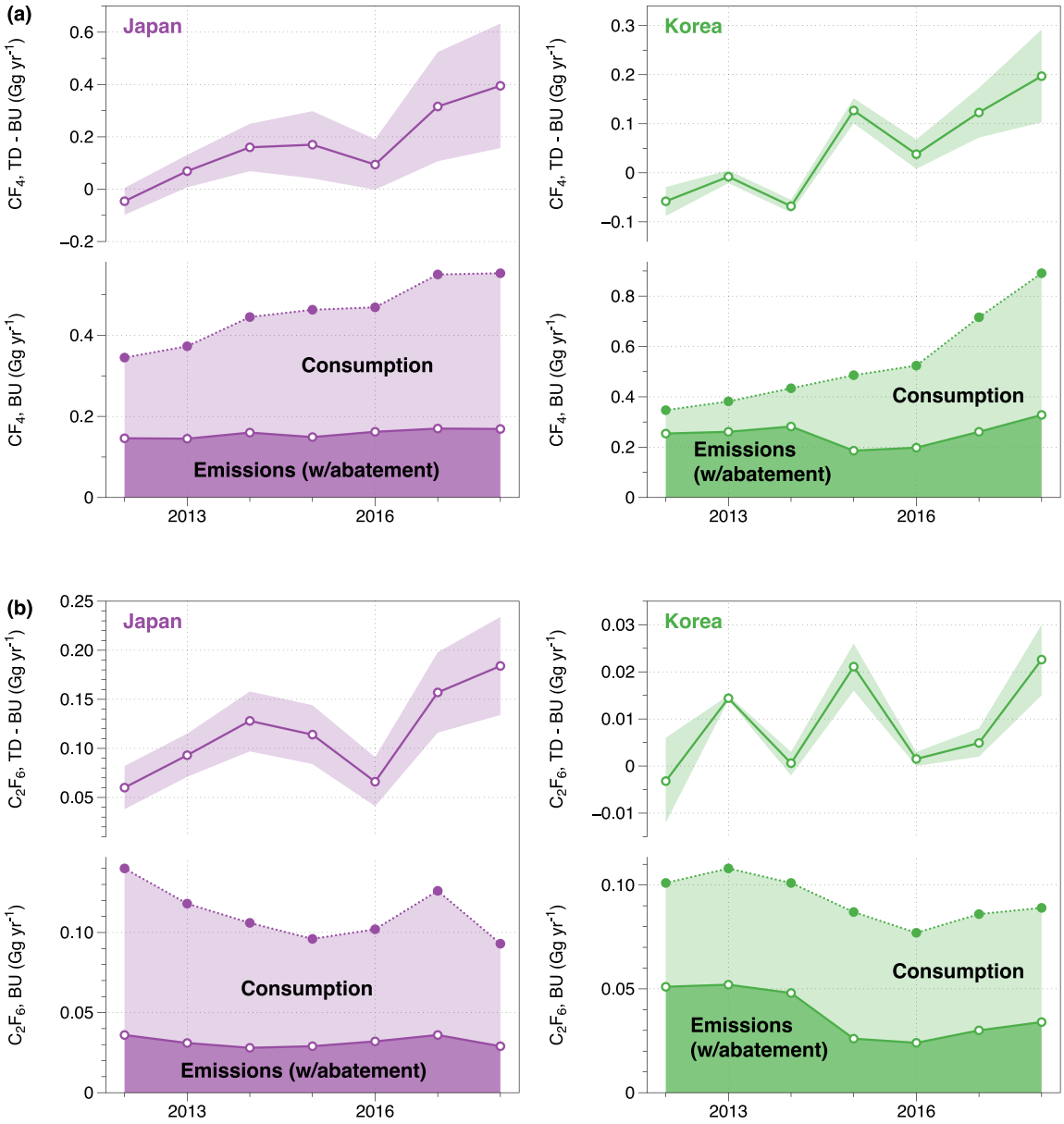

Figure 12. Japan (left) and Korea's (right) top-down emissions compared to bottom-up reported consumption emissions (accounting for estimated abatement) for (a) CF_4 and (b) C_2F_6.

7.4. Reassessing Global Top-Down Versus Bottom-Up Discrepancies

Does the upward revision of PFC emissions identified for East Asia in this study (i.e., modeled TD emissions in East Asia from Section 6 minus the reported BU for China's AL industry from Section 3.1, and NIR reported emissions for Japan and Korea from Section 3.2) close the gap in global TD and BU PFC emissions discussed in Section 2? The full uncertainties in this comparison are difficult to quantify, as the uncertainties in the reported BU emissions are difficult to define, and the modeled TD uncertainties as defined in our study may still underestimate the true uncertainties of the posterior results, as indicated by the significant year-to-year swings in the posterior emissions. Therefore, our assessment focuses on broad qualitative comparisons, with uncertainties based only on the TD results rather than on a full analysis of all uncertainties.

Our results for 2012–2018, where all the relevant BU reporting is available, are presented in Figure 13 and suggests that the upward revision of East Asian emissions identified in this study can help to significantly

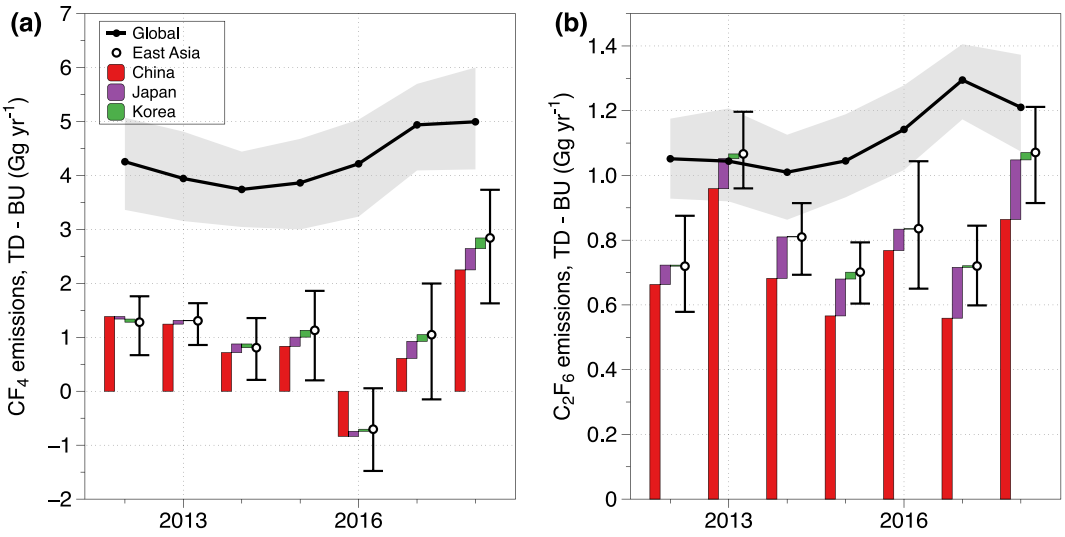

Figure 13. Emission differences between top-down (TD) and bottom-up estimates globally (black line) and for East Asia (totals in black dot, with a break-up of China (red), Japan (purple), and Korea (green) as offset stacked bars) for (a) CF_4 and (b) C_2F_6. Error bars represent uncertainties in the TD only and underestimate the total uncertainties in this comparison. Note that the regional discrepancy in some years is negative. See discussions in Section 5.4 for details.

close the gap in the global budget imbalance in CF_4 and C_2F_6. Overall, the increase in emissions TD versus BU in East Asia accounts for 25% and 77% of the global discrepancy in CF_4 and C_2F_6, respectively, on average over this period, but we note that the East Asian contributions for CF_4 increase to 32% of global emissions when excluding the large negative TD-BU difference in 2016.

Our results suggest that while accurate accounting of Chinese PFC emissions is important to understanding the global budget discrepancies for these compounds, the upward revision of emissions for China alone may not explain all of the missing emissions in the global BU to TD comparison. This is especially true for C_2F_6, where the upward revision of emissions for Japan are also found to make a significant contribution to the total East Asian upward revision. Beyond East Asia, Say et al. (2021) recently reported TD PFC emissions from northwest Europe, estimating total TD emissions of 0.13 Gg yr^{-1} (219% of the reported BU) and 0.036 Gg yr^{-1} (179% of the reported BU) that is, an increase above the reported BU emission estimates of 0.066 Gg yr^{-1} and 0.016 Gg yr^{-1}, averaged 2012–2018, for CF_4 and C_2F_6, respectively. For Australia, Dunse et al. (2019) estimated TD emissions over 2005–2017 for CF_4 (0.076 ± 0.024 Gg yr^{-1}) and C_2F_6 (0.008 ± 0.002 Gg yr^{-1}), finding that the reported BU emissions are lower by about 50% and 36%, and also that the TD versus BU discrepancy may be growing significantly since 2016. These findings are generally in line with our results in finding the reported BU emissions to be significantly underestimated at regional scales, but the relatively small emission magnitudes in these studies suggest that larger emissions and TD versus BU discrepancies could exist elsewhere. TD emission estimates are currently lacking in most other regions around the world, and extending observations and TD estimates will therefore be crucial to fully closing the global budget discrepancies for these PFCs.

8. Summary and Conclusions

Emissions of CF_4 and C_2F_6 from East Asia were estimated for 2008–2019 using a Bayesian inverse model (Thompson & Stohl, 2014) with atmospheric measurements at Gosan (Jeju Island, Korea). To assess the overall systematic uncertainties of our model framework, we used an ensemble of nine prior scenarios based on three different spatial distributions and three magnitudes with corresponding uncertainties, the range for which were determined through test inversion runs. The posterior results show overall significant error reductions and strong convergence at the annual scale, but also reveal some limitations of the single station inversion, including significant year-to-year variability in the results. This study therefore emphasizes our larger-scale modeled results, including the trends in totals for East Asia, and nationally for China, Japan, and Korea. We also note that significant uncertainties exist in our model results for western

China and eastern Japan, and emphasize the need for more observations that can help better resolve these uncertainties.

Our results suggest that the global increase in CF_4 emissions from 2012–2014 to 2017–2019 (Say et al., 2021) are likely driven by increased emissions from East Asia, however the evidence for East Asian emissions driving the global C_2F_6 increase during the same period is less certain. Our results nevertheless confirm the dominant role of East Asian emissions in the global PFC budgets.

Our modeled CF_4 emissions from China for recent years are well-matched with emissions reported for the Chinese aluminum industry (IAI, 2020; Bogle & Ottinger, 2020), suggesting that CF_4 emission characteristics from this industry may have improved over time, and also that CF_4 emissions from China's other industries may be relatively small. For C_2F_6, the proportional differences between our modeled Chinese emissions and those reported for their aluminum industry decrease with time at a rate similar to that of CF_4, however this difference still remains large. Our results for China suggest that aluminum industry emissions dominate CF_4 emissions, while C_2F_6 emissions are similarly large for their semiconductor and flat panel display industries, and emissions from other sectors such as rare earths may be relatively small.

In comparing our modeled emission results for Japan and Korea with reported semiconductor emissions for these countries (GIO, 2020; GIR, 2020), we find that CF_4 emissions more closely follow trends in increasing consumption than in emissions after abatement, suggesting that the 90% abatement efficiency typically assumed in the industry is unrealistic. This comparison for C_2F_6 shows a better overall match, although there may be additional C_2F_6 sources in Japan.

The underestimation of emissions in East Asia identified in this study can explain a significant portion of the global discrepancies between the PFC emissions reported from industry and government versus those derived from atmospheric observations, but significant gaps remain. Expanding regional atmospheric measurements and emissions analysis to currently undersampled regions of the world (Dunse et al., 2019; Say et al., 2021) will be crucial in fully understanding the budgets of these PFCs, and in ensuring that industry efforts to curb these emissions have the intended real-world impacts.

Data Availability Statement

CF_4 and C_2F_6 observations at Gosan used in this study are available at the AGAGE website (http://agage.mit.edu/data).

Acknowledgments
Support for contributions by J. Kim, J. Mühle, C. M. Harth, P. K. Salameh, R. Schmidt, and R. F. Weiss came from National Aeronautics and Space Administration (grant nos. NNX07AE89G, NNX07AF09G, and NNX07AE87G). R. Thompson acknowledges financial support from the European Commission, Horizon 2020 Framework Program (VERIFY, grant no. 776810). Support for contributions from H. Park, M.-K. Park, Y. Kim, and S. Park, and Gosan station operations was provided by National Research Foundation of Korea grant funded by the Korea government (No. 2020R1A2C3003774). S. Bogle and D. Ottinger are employees of the U.S. Environmental Protection Agency. The views expressed in this article are those of the author(s) and do not necessarily represent the views or policies of the U.S. Environmental Protection Agency.

References

Arnold, T., Harth, C. M., Mühle, J., Manning, A. J., Salameh, P. K., Kim, J., et al. (2013). Nitrogen trifluoride global emissions estimated from updated atmospheric measurements. *Proceedings of the National Academy of Sciences of the United States of America*, *110*(6), 201212346–201222034. https://doi.org/10.1073/pnas.1212346110

Arnold, T., Manning, A. J., Kim, J., Li, S., Webster, H., Thomson, D., et al. (2018). Inverse modelling of CF_4 and NF_3 emissions in East Asia. *Atmospheric Chemistry and Physics*, *18*(18), 13305–13320. https://doi.org/10.5194/acp-18-13305-2018

Arnold, T., Mühle, J., Salameh, P. K., Harth, C. M., Ivy, D. J., & Weiss, R. F. (2012). Automated measurement of nitrogen trifluoride in ambient air. *Analytical Chemistry*, *84*(11), 4798–4804. https://doi.org/10.1021/ac300373e

Bartos, S. C., Burton, C. S., Fraust, C. L., Illuzzi, F., Mocella, M. T., & Raoux, S. (2006). Electronics industry emissions. In *2006 IPCC guidelines for National Greenhouse Gas Inventories, Prepared by the National Greenhouse Gas Inventories Programme* (Vol. 3). Intergovernmental Panel on Climate Change (IPCC). Retrieved from http://www.ipcc-nggip.iges.or.jp

Bogle, S., & Ottinger, D. (2020). A comparison of bottom-up global emission estimates of PFCs from the electronics industry and atmospheric measurements. Presentation at the SESHA Virtual Symposium, June 24th, 2020.

Cai, B., Liu, H., Kou, F., Yang, Y., Yao, B., Chen, X., et al. (2018). Estimating perfluorocarbon emission factors for industrial rare earth metal electrolysis. *Resources, Conservation and Recycling*, *136*, 315–323. https://doi.org/10.1016/j.resconrec.2018.04.018

Center for International Earth Science Information Network (CIESIN) - Columbia University (2005). United Nations Food and Agriculture Programme (FAO), & Centro Internacional de Agricultura Tropical (CIAT) gridded population of the world, version 3 (GPWv3): Population count grid. *Future Estimates*. https://doi.org/10.7927/h42b8vzz

Chang, M. B., & Chang, J.-S. (2006). Abatement of PFCs from semiconductor manufacturing processes by nonthermal plasma technologies: A critical review. *Industrial & Engineering Chemistry Research*, *45*(12), 4101–4109. https://doi.org/10.1021/ie051227b

Choi, S., Hong, S. H., Lee, H. S., & Watanabe, T. (2012). A comparative study of air and nitrogen thermal plasmas for PFCs decomposition. *Chemical Engineering Journal*, *185–186*, 193–200. https://doi.org/10.1016/j.cej.2012.01.077

Czerniak, M. (2018). PFC emission reduction in the semiconductor industry. *Light Metals*, 1495–1498. https://doi.org/10.1007/978-3-319-72284-9_195

Czerniak, M. R., Tang, K., & Li, S.-N. (2007). Has the challenge of PFCs really been solved? *Semiconductor International*, *30*(11), 67–73.

Deeds, D. A., Vollmer, M. K., Kulongoski, J. T., Miller, B. R., Mühle, J., Harth, C. M., et al. (2008). Evidence for crustal degassing of CF_4 and SF_6 in Mojave Desert groundwaters. *Geochimica et Cosmochimica Acta*, *72*(4), 999–1013. https://doi.org/10.1016/j.gca.2007.11.027

Dunse, B. L., Derek, N., Fraser, P. J., Krummel, P. B., & Steele, L. P. (2019). Australian and global HFC, PFC, sulfur hexafluoride nitrogen trifluoride and sulfuryl fluoride emissions, Report prepared for Australian Government Department of the Environment and Energy (p. 33). Aspendale, Australia: CSIRO Oceans and Atmosphere. Retrieved from https://www.environment.gov.au/system/files/resources/a6d70dfd-24cf-4b3b-b819-ee8fe6d2ab69/files/report-sgg-2019.pdf

Fang, X., Park, S., Saito, T., Tunnicliffe, R., Ganesan, A. L., Rigby, M., et al. (2019). Rapid increase in ozone-depleting chloroform emissions from China. *Nature Geoscience*, *12*(2), 89–93. https://doi.org/10.1038/s41561-018-0278-2

Fang, X., Yao, B., Vollmer, M. K., Reimann, S., Liu, L., Chen, L., et al. (2019). Changes in HCFC emissions in China during 2011–2017. *Geophysical Research Letters*, *46*(16), 10034–10042. https://doi.org/10.1029/2019gl083169

Greenhouse Gas Inventory and Research Center of Korea (GIR) (2020). National greenhouse gas inventory report of Japan, CGER-Report. Available at https://unfccc.int/documents/223791

Greenhouse Gas Inventory Office of Japan (GIO) (2020). National greenhouse gas inventory report of Japan,CGER-Report. Available at https://unfccc.int/documents/223791

Harnisch, J., & Eisenhauer, A. (1998). Natural CF_4 and SF_6 on Earth. *Geophysical Research Letters*, *25*(13), 2401–2404. https://doi.org/10.1029/98GL01779

Hartmann, D. L., Tank, A. M. G. K., Rusticucci, M., Alexander, L. V., Bronnimann, S., Charabi, Y., et al. (2014). *Observations: Atmosphere and surface* (pp. 159–254). Cambridge. Cambridge University Press. https://doi.org/10.1017/cbo9781107415324.008

Holiday, R. D., & Henry, J. (1959). Anode polarization and fluorocarbon formation in aluminum reduction cells. *Industrial & Engineering Chemistry*, *51*(10), 1289–1292. https://doi.org/10.1021/ie50598a036

IC Insights (2011). Global wafer capacity (IC Insights). Available at http://www.icinsights.com/services/global-wafer-capacity/

International Aluminium Institute (IAI) (2020). Anode effect survey. Available at https://www.world-aluminium.org/statistics/

Kim, J., Fraser, P. J., Li, S., Mühle, J., Ganesan, A. L., Krummel, P. B., et al. (2014). Quantifying aluminum and semiconductor industry perfluorocarbon emissions from atmospheric measurements. *Geophysical Research Letters*, *41*(13), 4787–4794. https://doi.org/10.1002/2014gl059783

Kim, J., Li, S., Kim, K.-R., Stohl, A., Mühle, J., Kim, S.-K., et al. (2010). Regional atmospheric emissions determined from measurements at Jeju Island, Korea: Halogenated compounds from China. *Geophysical Research Letters*, *37*(12), L12801. https://doi.org/10.1029/2010gl043263

Li, S., Kim, J., Kim, K.-R., Mühle, J., Kim, S.-K., Park, M.-K., et al. (2011). Emissions of halogenated compounds in East Asia determined from measurements at Jeju Island, Korea. *Environmental Science & Technology*, *45*(13), 5668–5675. https://doi.org/10.1021/es104124k

Li, S., Park, S., Lee, J.-Y., Ha, K.-J., Park, M.-K., Jo, C. O., et al. (2018). Chemical evidence of inter-hemispheric air mass intrusion into the Northern Hemisphere mid-latitudes. *Scientific Reports*, *8*(1), 4669. https://doi.org/10.1038/s41598-018-22266-0

Marks, J., & Bayliss, C. (2012). GHG measurements and inventory for aluminum production. *Light Metals*, 805–808. https://doi.org/10.1007/978-3-319-48179-1_139

Marks, J., & Nunez, P. (2018). Updated factors for calculating PFC emissions from primary aluminum production. *Light Metals*, 1519–1525. https://doi.org/10.1007/978-3-319-72284-9_198

Miller, B. R., Weiss, R. F., Salameh, P. K., Tanhua, T., Greally, B., Mühle, J., & Simmonds, P. G. (2008). Medusa: A sample preconcentration and GC/MS detector system for in situ measurements of atmospheric trace halocarbons, hydrocarbons, and sulfur compounds. *Analytical Chemistry*, *80*(5), 1536–1545. https://doi.org/10.1021/ac702084k

Mühle, J., Ganesan, A. L., Miller, B. R., Salameh, P. K., Harth, C. M., Greally, B. R., et al. (2010). Perfluorocarbons in the global atmosphere: Tetrafluoromethane, hexafluoroethane, and octafluoropropane. *Atmospheric Chemistry and Physics*, *10*(11), 5145–5164. https://doi.org/10.5194/acp-10-5145-2010

Mühle, J., Trudinger, C. M., Western, L. M., Rigby, M., Vollmer, M. K., Park, S., et al. (2019). Perfluorocyclobutane (PFC-318, c -C_4F_8) in the global atmosphere. *Atmospheric Chemistry and Physics*, *19*(15), 10335–10359. https://doi.org/10.5194/acp-19-10335-2019

Myhre, G., Shindell, D., Bréon, F.-M., Collins, W., Fuglestvedt, J., Huang, J., et al. (2013). Anthropogenic and natural radiative forcing. In T. F. Stocker, D. Qin, G.-K. Plattner, M. Tignor, S. K. Allen, J. Doschung, et al. (Eds.), *Climate change 2013: The physical science basis. Contribution of working group I to the fifth assessment report of the intergovernmental panel on climate change* (pp. 659–740). Cambridge, UK and New York, USA. Cambridge University Press. https://doi.org/10.1017/cbo9781107415324.018

O'Doherty, S., Simmonds, P. G., Cunnold, D. M., Wang, H. J., Sturrock, G. A., Fraser, P. J., et al. (2001). In situ chloroform measurements at Advanced Global Atmospheric Gases Experiment atmospheric research stations from 1994 to 1998. *Journal of Geophysical Research*, *106*(D17), 20429–20444. https://doi.org/10.1029/2000jd900792

Ottinger, D. A., & Cai, B. (2019). Industrial processes and product use. In E. C. Buendia, K. Tanabe, A. Kranjc, J. Baasansuren, M. Fukuda, S. Ngarize, et al. (Eds.), *2019 Refinement to the 2006 IPCC guidelines for national greenhouse gas inventories* (Vol. 3). Switzerland. IPCC. Retrieved from https://www.ipcc-nggip.iges.or.jp/public/2019rf/vol3.html

Ou Yang, C.-F., Kam, S.-H., Liu, C.-H., Tzou, J., & Wang, J.-L. (2009). Assessment of removal efficiency of perfluorocompounds (PFCs) in a semiconductor fabrication plant by gas chromatography. *Chemosphere*, *76*(9), 1273–1277. https://doi.org/10.1016/j.chemosphere.2009.06.039

Park, S., Western, L. M., Saito, T., Redington, A. L., Henne, S., Fang, X., et al. (2021). A decline in emissions of CFC-11 and related chemicals from eastern China. *Nature*, *590*(7846), 433–437. https://doi.org/10.1038/s41586-021-03277-w

Pisso, I., Sollum, E., Grythe, H., Kristiansen, N. I., Cassiani, M., Eckhardt, S., et al. (2019). The Lagrangian particle dispersion model FLEXPART version 10.4. *Geoscientific Model Development*, *12*(12), 4955–4997. https://doi.org/10.5194/gmd-12-4955-2019

Prinn, R. G., Weiss, R. F., Arduini, J., Arnold, T., DeWitt, H. L., Fraser, P. J., et al. (2018). History of chemically and radiatively important atmospheric gases from the Advanced Global Atmospheric Gases Experiment (AGAGE). *Earth System Science Data*, *10*(2), 985–1018. https://doi.org/10.5194/essd-10-985-2018

Rigby, M., Park, S., Saito, T., Western, L. M., Redington, A. L., Fang, X., et al. (2019). Increase in CFC-11 emissions from eastern China based on atmospheric observations. *Nature*, *569*(7757), 546–550. https://doi.org/10.1038/s41586-019-1193-4

Rodgers, C. D. (2000). Inverse methods for atmospheric sounding, theory and practice. *World Scientific*. https://doi.org/10.1142/3171

Saha, S., Moorthi, S., Pan, H. L., Wu, X., Wang, J., Nadiga, S., et al. (2010). NCEP Climate Forecast System Reanalysis (CFSR) 6-hourly products, Research data archive at the National Center for Atmospheric Research, Computational and Information Systems Laboratory. Boulder, CO. https://doi.org/10.5065/D69K487J

Saha, S., Moorthi, S., Wu, X., Wang, J., Nadiga, S., Tripp, P., & Becker, E. (2011). NCEP Climate Forecast System version 2 (CFSv2) 6-hourly products, Research data archive at the National Center for Atmospheric Research, Computational and Information Systems Laboratory. Boulder, CO. https://doi.org/10.5065/D61C1TXF

Saito, T., Yokouchi, Y., Stohl, A., Taguchi, S., & Mukai, H. (2010). Large emissions of perfluorocarbons in East Asia deduced from continuous atmospheric measurements. *Environmental Science & Technology*, *44*(11), 4089–4095. https://doi.org/10.1021/es1001488

Say, D., Manning, A. J., Western, L. M., Young, D., Wisher, A., Rigby, M., et al. (2021). Global trends and European emissions of tetrafluoromethane (CF_4), hexafluoroethane (C_2F_6) and octafluoropropane (C_3F_8). *Atmospheric Chemistry and Physics*, *21*(3), 2149–2164. https://doi.org/10.5194/acp-21-2149-2021

Smith, J. (2020). To revive rare-earth industry, U.S. looks to the Mojave. Los Angeles Times. Available at https://www.latimes.com/business/story/2020-09-25/rare-earths-california-mojave

Stohl, A., Kim, J., Li, S., O'Doherty, S., Mühle, J., Salameh, P. K., et al. (2010). Hydrochlorofluorocarbon and hydrofluorocarbon emissions in East Asia determined by inverse modeling. *Atmospheric Chemistry and Physics*, *10*(8), 3545–3560. https://doi.org/10.5194/acp-10-3545-2010

Taberaux, A. T. (1994). Anode effects, PFCs, global warming, and the aluminum industry. *JOM*, *46*, 30–34.

Thompson, R. L., & Stohl, A. (2014). FLEXINVERT: An atmospheric Bayesian inversion framework for determining surface fluxes of trace species using an optimized grid. *Geoscientific Model Development*, *7*(5), 2223–2242. https://doi.org/10.5194/gmd-7-2223-2014

Trudinger, C. M., Fraser, P. J., Etheridge, D. M., Sturges, W. T., Vollmer, M. K., Rigby, M., et al. (2016). Atmospheric abundance and global emissions of perfluorocarbons CF_4, C_2F_6 and C_3F_8 since 1800 inferred from ice core, firn, air archive and in situ measurements. *Atmospheric Chemistry and Physics*, *16*(18), 11733–11754. https://doi.org/10.5194/acp-16-11733-2016

Vogel, H., & Friedrich, B. (2015). Development and research trends of the Neodymium electrolysis - A literature review. *Proceedings of EMC*, *1*. https://doi.org/10.2307/41411006

Vogel, H., & Friedrich, B. (2018). An estimation of PFC emission by rare earth electrolysis. In M. O. (Ed.), *Light metals 2018* (pp. 1507–1517). Cham. Springer. https://doi.org/10.1007/978-3-319-72284-9_197

Wong, D. S., Fraser, P. J., Lavoie, P., & Kim, J. (2015). PFC emissions from detected versus nondetected anode effects in the aluminum industry. *JOM*, *67*(2), 1–12. https://doi.org/10.1007/s11837-014-1265-8

World Semiconductor Council (WSC) (2020). *Joint statement of the 24th meeting of the world semiconductor Council (WSC)*. Available at http://www.semiconductorcouncil.org/public-documents/joint-statements-from-prior-wsc-meetings/